

**University of Michigan**  
**Project Title**  
**Cargo Balancing Expandable Exploration Platform (Cargo-BEEP)**

**Team Members**

*Gianna Belmont* - Undergraduate Student, Electrical Eng, Foreign National  
*Justin Boverhof* - Undergraduate Student, Robotics  
*Evan Branson* - Graduate Student, Robotics  
*Jason Brown* - Undergraduate Student, Aerospace Eng. and Robotics  
*Hannah Cherry* - Undergraduate Student, Aerospace Eng.  
*Ryan Foster* - PhD Student, Aerospace Eng.  
*Lucille Gorbe* - Undergraduate Student, Climate and Space Science and Eng.  
*Kimberly Gurwin* - Undergraduate Student, Robotics  
*Tyler Nanoff* - Graduate Student, Mechanical Engineering  
*Salem Loucks* - Undergraduate Student, Computer Science Eng.  
*Timothy Mellema* - Undergraduate Student, Aerospace Eng  
*Rahul Nair* - Graduate Student, Mechanical Eng.  
*Christopher Packard* - Undergraduate Student, Aerospace Eng.  
*Michael Robinson* - Undergraduate Student, Robotics  
*Avery Sanchez* - Undergraduate Student, Environmental Engineering  
*Raven St. Clair* - Undergraduate Student, Aerospace Eng. and Astrophysics  
*Shai Toledano* - Undergraduate Student, Aerospace Eng. and Astrophysics  
*Juan Vega* - Undergraduate Student, Aerospace Eng.  
*Luke Weaver* - Undergraduate Student, Computer Eng.

**Faculty Advisors**

*John Shaw*, Professor in Aerospace Eng. Dept., Primary Faculty Advisor  
*Elliott J. Rouse*, Professor in Robotics Eng. Dept., Faculty Co-Advisor

**Space Grant Affiliation**

Michigan Space Grant Consortium. Prof. Mark Moldwin, Director, University of Michigan Email and Phone: [mispacegrant@umich.edu](mailto:mispacegrant@umich.edu), (734) 936-2698 | Director Email: [mmoldwin@umich.edu](mailto:mmoldwin@umich.edu)

Faculty Signature: \_\_\_\_\_

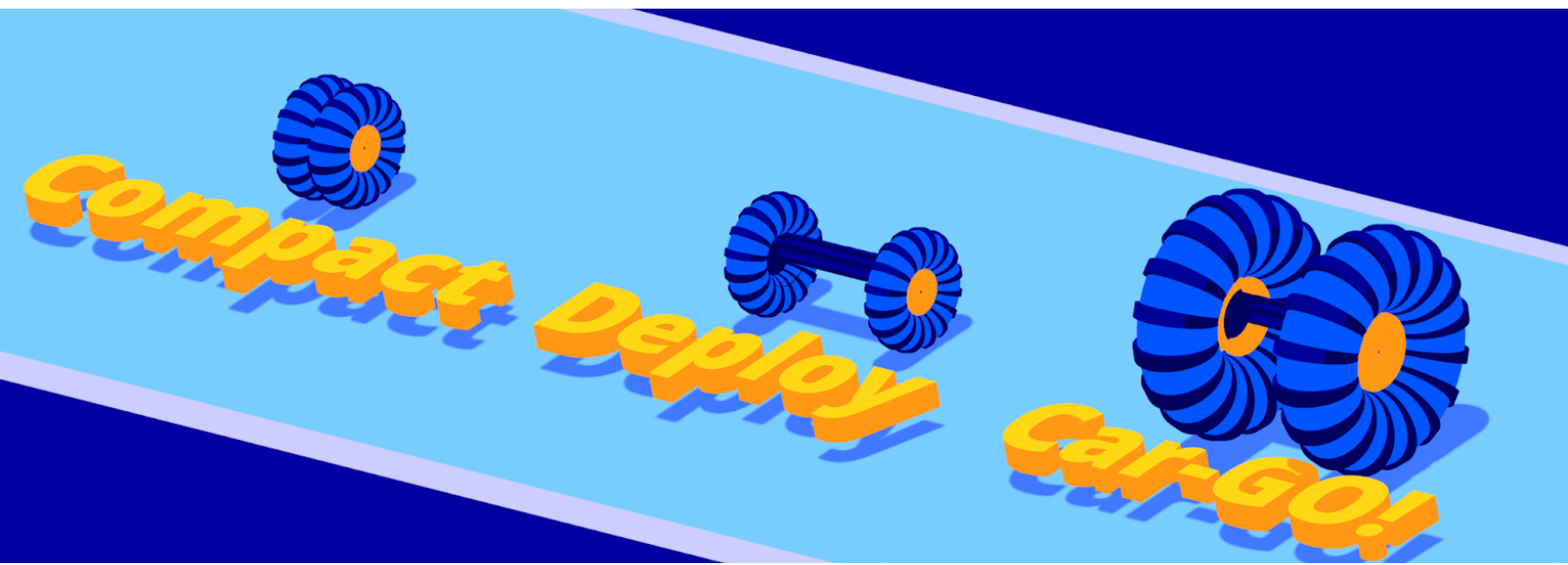
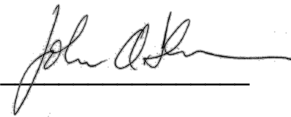


## Table of Contents

<b>1.0 Quad Chart.....</b>	<b>3</b>
<b>2.0 Executive Summary.....</b>	<b>4</b>
<b>3.0 Problem Statement.....</b>	<b>5</b>
<b>4.0 Project Description.....</b>	<b>6</b>
4.1 Wheels and Materials.....	6
4.2 Deployable Chassis System.....	7
4.2.1 Inflatable Body.....	7
4.2.3 Cargo Bed.....	7
4.3 Controls System.....	7
4.4 Life Cycle Analysis.....	8
4.5 Concept Integration and Operation.....	8
4.6 Potential Stakeholders.....	8
<b>5.0 Design and Analysis.....</b>	<b>9</b>
5.1 Wheels and Materials.....	9
5.1.1 Hermetic Layer.....	9
5.1.2 Gasket.....	9
5.1.3 Fill system.....	10
5.1.4 Restraint Layer.....	10
5.1.5 Abrasion Layer.....	10
5.2 Deployable Chassis System.....	11
5.2.1 Inflatable Body.....	11
5.2.2 Fill System.....	11
5.2.3 Collapsible Rods.....	11
5.3 Controls System.....	12
5.3.1 Electronics.....	12
5.3.2 Software.....	12
5.4 Thermal Analysis.....	13
5.5 Structural analysis.....	13
5.6 Deployment Mechanisms and Operations.....	14
5.7 Risk Management.....	15
<b>6.0 Verification Testing on Earth.....</b>	<b>16</b>
6.1 Wheel Dynamics and Material Usage.....	16
6.1.1 Traction.....	16
6.1.2 Puncture Testing.....	17
6.2 Body Deployment Testing.....	19
6.3 Controls System.....	19
6.3.1 PID Tuning.....	19
6.3.2 Wave Field Testing.....	20
6.4 Thermal Vacuum Testing.....	20
<b>7.0 Path to Flight.....</b>	<b>22</b>

7.1 Path to implementation.....	22
7.1.1 Wheels.....	22
7.1.2 Body.....	22
7.1.3 Controls System.....	23
7.2 Continued Development.....	23
7.2.1 Wheels.....	23
7.2.3 Controls.....	23
<b>8.0 Project Management.....</b>	<b>24</b>
8.1 Leadership.....	24
8.2 Schedule.....	24
8.2.1 Mid-Project Report Schedule.....	24
8.2.2 Schedule Changes.....	25
8.2.3 Schedule Difficulties.....	26
8.3 Budget.....	26
<b>Appendix A: Conservative Thermal Analysis.....</b>	<b>27</b>
<b>Appendix B: Structural Analysis.....</b>	<b>35</b>
Appendix B.1 Static Load From Cargo.....	35
Appendix B.2 Torsional load from motors.....	37
<b>Appendix C: References.....</b>	<b>38</b>

## 1.0 Quad Chart



# Cargo Balancing Expandable Exploration Platform (Cargo-BEEP)



### Concept Synopsis:

The Cargo Balancing Expandable Exploration Platform (Cargo-BEEP) is a self-deploying inflatable vehicle. It is intended to be easily carried by an astronaut when stowed and then deployed to transport cargo.

### Technical Requirements

1. Self-deployment of body and wheels
2. Able to carry 250kg of cargo
3. Resistance to lunar environment (abrasion, thermal, etc)
4. Capable of both autonomous and controlled operation
5. Capable of traversing inclines of up to 45 degrees
6. Able to continuously operate for at least an hour

### Innovations

Our two-wheeled inflatable vehicle design allows for unparalleled compactability while minimizing complexity and moving parts.

#### Inflatable Body

- Allows the compact form to deploy to a full-sized vehicle.
- Doubles as the primary load-bearing component for cargo.
- Demonstrates the use of inflatables for deployment of dynamic and load-bearing systems, transferable to inflatable habitats and future vehicles.

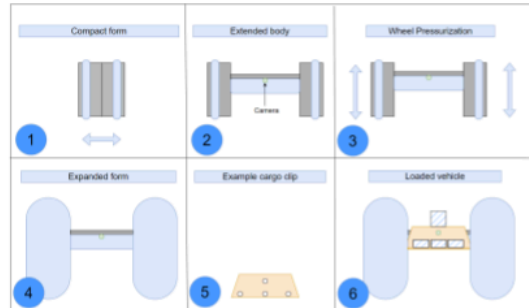
#### Wheel

- Inflates from compact form to 3x original diameter, providing clearance to transport cargo on rough lunar terrain.
- Self-contained motor and inflation mechanisms are highly adaptable to other lunar vehicles.
- 3-layer wheel provides durability and collapsibility

#### Controls

- Self-balancing control system allows for the use of two-wheeled systems for cargo and personnel transport on the lunar surface.

### Image



### Verification Testing Results & Conclusions

#### Puncture Testing

- Materials for abrasion layer tested against slashing, puncture, abrasion and heat, determining ballistic nylon to be most resistant to lunar conditions.

#### Wheel Deployment Testing

- Inflated 2/3 scale wheel to 20 psi and encountered persistent leakage issues, primarily along the seam. Different material or sealing method required.

#### Main Body Deployment Testing

- Demonstrated the telescoping rod deployment system with the inflation of the main body to 15 psi.
- More effective stowage would require a thinner restraint layer and lower-tolerance telescoping rods.

#### Controls Testing

- Tested a prototype with PID control software on hills and sand, climbing inclines greater than 45 degrees, and remotely stopping the robot. Validated our control system design.

## 2.0 Executive Summary

Cargo-BEEP is designed to fulfill low-priority lunar transportation and exploration needs where sending mission-critical rovers would be risky or logistically complicated. The LTV is an excellent platform for trips far from Artemis Base Camp, but it is overqualified to handle smaller tasks closer to home. Its high performance comes with a high logistical and financial cost that makes it less than ideal for spontaneous or potentially damaging maneuvers. Cargo-BEEP offers a low cost and thus low risk alternative for such missions. This makes it ideal to carry tools, sensors, and samples around Artemis Base Camp.

Cargo-BEEP will utilize inflatables to minimize size, weight, and power for smaller-scale operations. Cargo-BEEP's inflatable wheels and chassis allow it to expand from a compact storage profile into its operational configuration with a volume expansion ratio of approximately 5:1. Cargo-BEEP's high ground clearance allows it to navigate otherwise challenging terrain, and its cargo capacity of 300 kg and range of 10 km on the lunar surface allows it to carry ample gear and supplies to support astronaut excursions.

Cargo-BEEP will expand the possibilities for lunar exploration by providing an alternative to traditional lunar vehicle tires. Our inflatable wheel design minimizes size and weight while retaining the functionality of traditional tires. This innovation could save cost and mass on future missions. Low pressure, high surface area inflated wheels also offer additional robustness against sharp or uneven terrain not possible for their rigid counterparts. Drawing lessons from off-road and two-wheeled vehicles on Earth, Cargo-BEEP offers unique applications for the lunar environment. It demonstrates compact packaging and deployment with inflatable wheels in a way that has yet to be explored on the lunar surface.

Cargo-BEEP's inflatable cargo platform demonstrates two novel applications of inflatable technology by serving as both the deployment mechanism and primary load-bearing component of the chassis. The inflatable body pushes the wheels apart to expand the rover and provide axial rigidity, while collapsing rods expand passively with the body to provide torsional rigidity. After expansion, the body carries the weight of an externally attached cargo bed and cargo, while the rods stabilize the bed against lateral slip. This provides a simple mechanism for deployment with no electronics and relatively few steps and points of failure.

Cargo-BEEP's control system is an innovative application of Segway-style robots in a lunar environment. Cargo-BEEP implements an inverted-pendulum control system, which manages the system's inherent instability. It uses a state-based PID closed loop controller so the robot can maintain knowledge of where it is and adjust for both previous and future error. This provides state tracking data and can be used with more complex navigation and GPS systems.

### 3.0 Problem Statement

The ground vehicles of the Artemis program will be highly robust and highly capable; however, some missions may be too risky or low-priority to utilize these expensive and hard-to-replace resources. Cargo-BEEP (Cargo Balancing Expandable Exploration Platform) provides low cost, low weight exploration and transportation capabilities for use cases where utilizing larger, more expensive vehicles would be too risky or time-consuming. In *Lunar Mobility Drivers and Needs* and *Lunar Surface Cargo*, NASA outlined the mobility requirements for the success of the Artemis program[1][2]. The 4.0 km distance between the In-Situ Resource Utilization (ISRU) mining site and processing site is of principal interest to us.

Cargo-BEEP is a two-wheeled, deployable, inflatable, semi-autonomous rover capable of carrying up to 300 kg of cargo to and from these sites. We define the mission for Cargo-BEEP as 30 minutes of driving at 5 mph, followed by 3-5 hours of idling while astronauts perform tasks, followed by 30 min of driving at 5 mph back to the base site with 300 kg of cargo onboard. Cargo-BEEP is a two-wheeled, single-axle rover, which functions similarly to a Segway post-inflation. The single-axle minimizes volume when compared to dual-axle designs. Tests of our prototype have demonstrated that the rover can easily carry 50 kg of cargo at inclines of 12°, and could be modified for far higher loads. A load capacity of 50 kg on Earth corresponds to approximately 300 kg of load under lunar gravity. Given the lower cost, size, and weight of Cargo-BEEP, we believe sending multiple rovers with Artemis would be cost-effective. A network of low-cost rovers to haul materials and explore risky locations could supplement larger rovers' mission profiles. The compacted form of Cargo-BEEP can be carried by larger rovers, increasing the operational freedom of lunar excursions. To accomplish these tasks most effectively, our key performance parameters are cargo capacity, range, and power.

#### 4.0 Project Description

Cargo-BEEP is divided into three subsystems: the wheels, the deployable chassis, and robotic controls. The physical subsystems are illustrated in Figure 1. The wheel subsystem consists of the wheel rim and the inflatable softgoods wheel. The deployable chassis subsystem consists of an inflatable body that both supports the load of the cargo and deploys the expandable chassis, as well as collapsible rods for torsional resistance and additional structural support. The wheel subsystem includes the electronics and fluid bays, which house the motors, batteries, electronics, and inflation systems, while also interfacing between the wheel and body subsystem. The wheel is connected to the electronics bay via a shaft, the collapsible rods are welded to the back of the electronics bay, and the inflatable body is attached to and deploys from the recessed inner wheel hub faces. In compact form, the softgoods wheels fold against the wheel rim, the body folds into a recess in the fluids and electronics bays (e-bays), and the collapsible rods nest inside each other. The wheel rim mostly encapsulates the fluids bay when compact, with a 4 inch gap open to allow access to fill lines. A comparison of the compact vs. expanded system is illustrated in Figure 1.

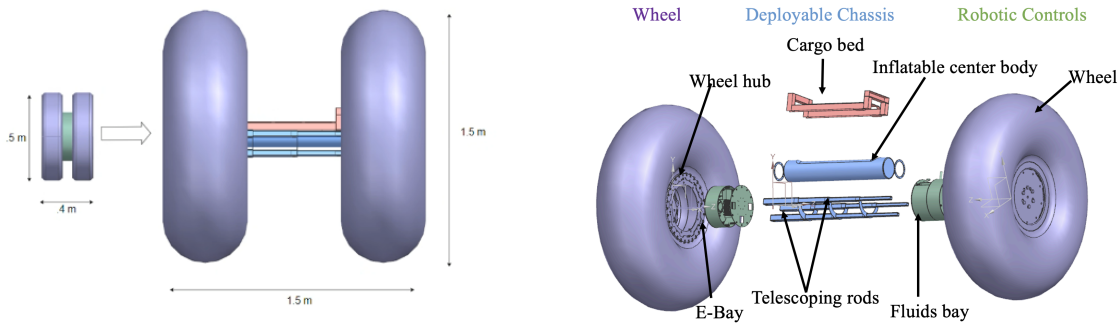


**Figure 1.** (right) A comparison between the compact and expanded states of Cargo-BEEP. (left) An exploded view of the Cargo-BEEP assembly. Note that the cargo bed is placed after deployment.

#### 4.1 Wheels and Materials



**Figure 2.** Wheel inflated with fill system and all layers.

The wheel hub assembly consists of a rim, softgoods wheel layers, and a set of plates and fasteners that bolt the wheel layers together. These plates allowed us to modify the geometry of the COTS (commercial off-the-shelf) wheel hub for integrating the softgood components.

The inflatable portion of the wheels are composed of three layers: the hermetic layer, the restraint layer, and the abrasive layer. The hermetic layer is a gas barrier. The restraint layer contains expansion. The abrasion layer is used for environmental protection, primarily against ultraviolet radiation, induced material degradation, and lunar dust ingress. We integrated softgoods components working outwards, starting with the hermetic layer and ending with the abrasion layer.

## 4.2 Deployable Chassis System

The deployable chassis system drives the expansion of the robot from the collapsed state to the fully expanded state and provides support to cargo. It consists of the inflatable body, the collapsible rods, the fill system, and the cargo bed. This system was planned to be integrated into the full scale robot, due to time constraints we settled on creating a deployment prototype that would simulate the expansion process. The prototype weighs approximately 9.4 kg, 7.4 kg for the rig, and 2.0 kg for the hermetic and restraint layers. The rig expands from a collapsed 0.57 m length to a full 1 m length. Additional expandability can be gained by adding more and/or longer collapsing rods and lengthening the inflatable.

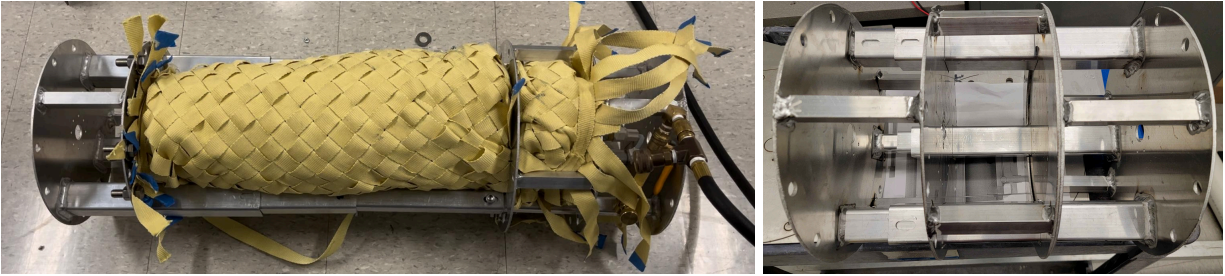


**Figure 3.** (Left) Full Deployment Prototype. Demonstrates the fill system, woven restraint layer, collapsing rods, and hermetic layer in the expanded state. (Right) Telescoping rods with brackets for the deployment rig. The ends have been welded to a plate to approximate the electronics bay

### 4.2.1 Inflatable Body

The body consists of 3 layers, a hermetic layer that holds pressure, a restraint layer that absorbs the loads on the hermetic layer and guides the shape, and an abrasion resistant layer. As the body is pressurized, it presses against the flat faces of the electronics bays, pushing the electronics bays apart, which expands the robot. The body would be inflated to rigidity. Initial tests verified this mechanism to 35 psi. 15 psi ( $1.03 \times 10^5$  Pa) was used for the last prototype due to difficulties with the selected hermetic layer. The body starts collapsed and straightens out as it is pressurized.

### 4.2.2 Collapsing Rods

The collapsing rods are the main supporting structure of the robot. For the mid-project report, we used two parallel rods that locked using spring pins. In the new model, they are a set of 3 square aluminum collapsing rods with four 10-inch segments on each rod arranged in a triangular pattern. Each set has a bracket that prevents twist and holds joining Kevlar straps. The end segments are welded to the electronics bays. Each rod also has two pill-shaped slots on each end that punch through both sides of each rod for locking the deployed configuration. A more advanced rod-locking approach is described in Section 7.2.2. Due to manufacturing issues, the fill system and this lip ended up on the wrong side and impeded collapse. The length and number of rods can be varied to achieve different expansion lengths.

### 4.2.3 Cargo Bed

The cargo bed provides a flat surface for cargo to rest on, and in our prototype it was also designed to lock the robot into its deployed configuration (rather than a more complex locking mechanism internal to the rods). It consists of a metal frame and a central metal plate with straps that rests on the body so it can help support cargo loads. Due to time constraints we were unable to finish constructing the cargo bed.

## 4.3 Controls System

The goal of the controls prototype was to develop and demonstrate a control algorithm that would allow Cargo-BEEP to balance and move safely after deployment. After inflation, Cargo-BEEP becomes a “inverted pendulum on a cart” robot, like a Segway. On Cargo-BEEP, the deployable chassis system and payload act as the pendulum, and the robot manipulates the lean angle of the body to create linear acceleration. This style of robot is inherently unstable because the system is balanced around an unstable equilibrium point. Without a control system, any disturbance to the pendulum will cause it to fall away from the equilibrium point. Therefore, Segway-style robots employ a closed-loop feedback controller to maintain stability around the unstable point. The robot’s balance can be described by four controllable



variables: angular position, angular velocity, linear position, and linear velocity. Proper control of the body's angular position ensures the system is always balanced.

Through experimental testing and secondary research, we determined that a PID (proportional-integral-derivative) controller or a state-state based control system such as LQR (linear-quadratic regulator) were the best options. The advantage of the PID controller was that it was easier to implement, however it does not account for every possible state of the robot. We decided to move forward with PID, as our team had limited experience with LQR.

#### **4.4 Life Cycle Analysis**

The batteries of Cargo-BEEP are rechargeable, and most rigid components do not experience high loads. It is therefore likely that Cargo-BEEP's lifetime will be limited by the integrity of the wheels. The outer abrasion layer of the wheel can be replaced with minimum effort. The restraint layer was made with Kevlar in the prototype; Vectran would provide better creep resistance. While the restraint layer would creep with time, it is unlikely it would fail as the pressures it is subjected to are a negligible fraction of the capabilities. Currently, the most likely failure is the hermetic layer due to poor material choice. The prototype design is suboptimal due to time and cost constraints, with a makeshift gasket and a very small contact area for sealing against the edge of a COTS wheel rim. Additionally, the cost and lead times of quality bladder materials, such as those used in TransHab, were prohibitive for our team. With proper gasket design, a secondary adhesive seal, and an appropriate selection of material for the bladder layer, we believe this prototype could be designed to function for several missions. Performing cyclic testing until failure was out-of-scope for our team due to time constraints.

#### **4.5 Concept Integration and Operation**

The completed Cargo-BEEP system would have the ability to transport cargo over at least 10 km in lunar environments. An external tank of inert gas, landed separately from Cargo-BEEP, would be used to deploy the inflatable system. These gas tanks can be carried with Cargo-BEEP on the LTV for deployment at mining sites as well as at the Artemis Base Camp. The system will also require access to electrical power in order to recharge its batteries. Therefore, a fluid and electrical interface must be integrated in the chassis of the system. As the cargo bed is modular, it will require different interfaces depending on the category. For example, a surface sample collection module would need to be accessible by astronauts in EVA suits. Likewise an ISRU transport module would need a fluid transfer interface in order to carry liquid water. It is preferable that these interfaces would be standardized across mission hardware, increasing interoperability.

#### **4.6 Potential Stakeholders**

Cargo-BEEP develops two major new technologies: compact inflatable wheels and inflation for the deployment of rigid systems. Compact inflatable wheels can save both mass and volume compared to traditional wheels. They are more scalable, with the mass of inflatable wheels scaling with volume far slower than any traditional wheel. Thus, any future lunar vehicles that require large wheels, such as mobile habitats, construction equipment, and mining vehicles could greatly benefit from our inflatable wheel technology. Additionally, a fleet of compact and cheap cargo-carrying robots like Cargo-BEEP could be used to transport mined materials like a conveyor belt while more permanent lunar infrastructure is being developed.

Inflatables, such as the one we developed for our inflatable body, could be used as a deployment mechanism and load-bearing component for other rigid or semi-rigid systems such as habitats and emergency radio transmitters. Thus, potential stakeholders for Cargo-BEEP's technology include the future lunar-mining industry, lunar construction industry, and the government.

## 5.0 Design and Analysis

This section highlights the manufacturing stage and post-manufacturing analysis that we have completed since the mid-project report, including manufacturing techniques and preliminary testing.

### 5.1 Wheels and Materials

All wheel layers are joined to the wheel hub. This allows the torque provided from a motor to counteract all of the torque received from the chassis to balance out our acceleration. We are assuming minimal slip between the layers against each other. A breakdown of joining techniques is located in Table 1.

Layers	Requirements (if any)	Joining Technique
Hermetic to hub	Cannot be punctured	Pressure fit with fabric and teflon gasket between metal plates.
Restraint to hub	Must not compromise structural integrity of restraint	Wrapped modified clevis roller design with wire. Located on the outer edge of the restraint ring.
Abrasion to hub	None	Wrapped around and screwed into the restraint ring.

**Table 1.** Joining Techniques for each layer of the inflatable systems

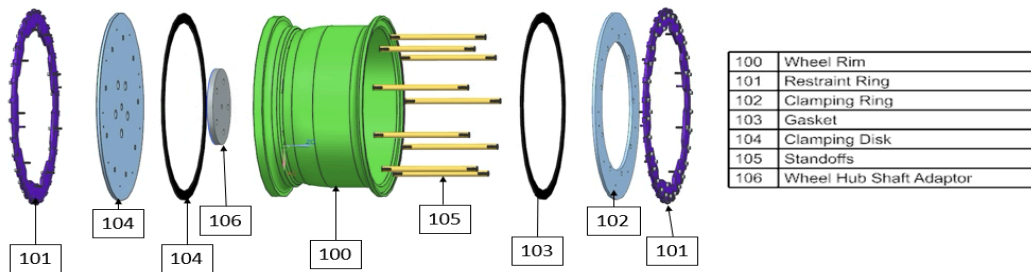


**Figure 4.** Exploded View of the wheel hub assembly with labels.

#### 5.1.1 Hermetic Layer

The hermetic layer maintains a gas barrier and is oversized to prevent it from sustaining pressure loads. Our chosen material was originally polyurethane coated Nylon due to extensive aerospace use history. Through permeability and pressure testing we determined we were unable to seal the nylon with available technology, so 10 mil Polyethylene Terephthalate (PET), which had been used in an earlier prototype of the deployment chassis, was chosen as a contingency. The hermetic layer is a non-loadbearing gas barrier; pressure loads are supported by the restraint layer. The hermetic layer was attached to the wheel hub via a gasket and aluminum clamping ring, and pressure was maintained between the tire rim and the fabric. After repeated pressure cycles with multiple materials we have determined that heat seals are generally the failure point in hermetic layers of this design.

#### 5.1.2 Gasket

The material interface of the hermetic layer is composed of a 16 in gasket formed with ePTFE (expanded Teflon) tape. ePTFE was chosen due to it having similar properties to PTFE (Teflon) while being less susceptible to deformation. The sealing interfaces are the COTS wheel rim and 0.25 in aluminum ring. Due to the geometry of the COTS wheel, the gasket's fasteners are connected to metal rods that run throughout the height of the wheel rim. The aluminum rings on both sides of the wheel are compressed around the metal rods, forming an airtight seal. The proposed design for flight would utilize a 16" ID ePTFE gasket cut from ePTFE sheets. This was not implemented on the prototype due to increased manufacturing costs. The sealing surfaces would be the designed wheel rim and clamping ring illustrated in Figure 5. The hermetic layer material would then be folded over the wheel rim and sealed against the wall with RSV silicone or a material-compatible sealant as a redundant measure to protect against rapid decompression in the event of gasket failure.

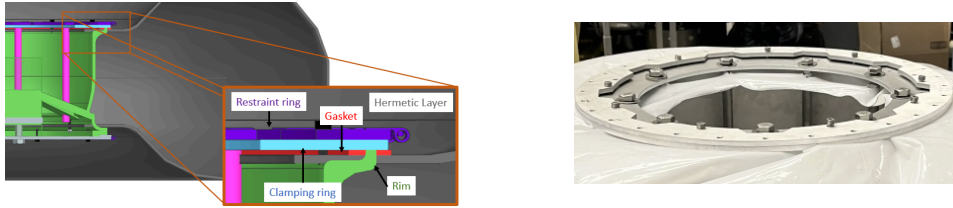


**Figure 5.** (Left) CAD layout of gasket implementation. (Right) Actual manufactured gasket.

### 5.1.3 Fill system

The wheels are filled through a NPT tapped hole in the rim. A PTFE hose is connected to the hole and extends out. Figure 6. shows a plumbing and integration diagram of the wheel fill system.

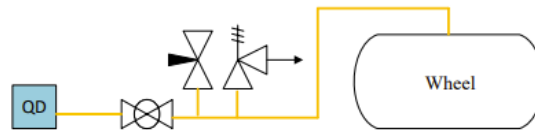


**Figure 6.** Wheel plumbing and integration diagram. Pressurant flows through the quick disconnect to the ball valve. It releases pressure via the needle valve and relief valve.

### 5.1.4 Restraint Layer

We initially experimented with different weave patterns using 1 inch satin ribbon. Patterns included: 90 degrees around a full torus, 45 degrees around a full torus, 45 degrees around a full torus double wrapped, and an open torus completed on the inside by the wheel rim, as illustrated in Figure 5.

The open torus design was chosen to avoid damaging the pressure inlet during motion. Future work would include incorporating radial straps such as the pattern used in the TransHab prototype for good coverage on the outer circumference [3]. Better coverage would also decrease the drift of the straps away from their original locations.

The restraint layer was woven around a scaffold consisting of a pool floaty and wheel hub components, and then transferred to the finalized wheel hub assembly. We followed a 45 degree helix pattern that required only joining Kevlar straps onto the end of the preceding strap once we ran out of material. In these sections, we used the diamond stitch pattern that NASA recommended for weaving 1 inch straps of material together [4]. We used a back stitch along the “double tapered diamond stitch” in the locations where we were adding new Kevlar straps to the ends of existing ones.

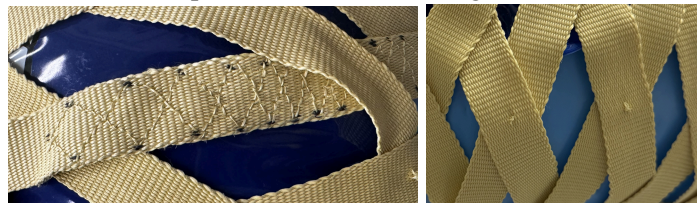


**Figure 7.** (Left) Diamond Stitch on straps for connecting ends together. (Right) Sewn center Xs sewn to reduce restraint layer shifting.

As seen in Figure 7, we also employed a small stitch in the center of the Xs of the pattern to prevent the Kevlar straps from slipping axially during motion. We chose Kevlar due to its previous flight history, existing industry contact, and it’s rated 3000 lb tensile strength [5].

### 5.1.5 Abrasion Layer

The abrasion layer is a protective fabric layer over the restraint layer. We chose ballistic nylon as our material due to the results from material testing (see section 6.1.2). A thermal analysis (Section 5.4) proved that a thermal layer was not necessary.

## 5.2 Deployable Chassis System

The inflatable body drives the expansion of the rover. It functions as a long linear actuator, driving the two wheels apart from one another. It is composed of 3 layers, mimicking the design of the wheels. The layered structure is an improvement over the 1/3 scale design we used during the mid-project report, as that was a Mylar tube attached to the hubs via hose clamps and sealed with an o-ring.

### 5.2.1 Inflatable Body

The hermetic layer is a 1 m long, 0.15 m diameter cylinder, made from PET plastic. It is sealed on 3 sides, and has a small hole where the gasket interfaces with the fill system. Aside from this attachment point, the hermetic layer will be completely separated from the restraint layer. Similar to the wheel, the hermetic layer is oversized such that the restraint layer bears all pressure loads.



**Figure 8.** (Left) Hermetic layer. Shows the PTFE gasket seal and the PET plastic layer heat sealed around it. (Right) Restraint layer during fabrication. Note the cross-hatched “finger trap” design that will pull taut as the robot expands.

The restraint layer provides the strength of the body, supporting the hermetic layer. The restraint layer consists of long strips of Kevlar woven in a large finger trap pattern, with two layers woven together at a 45° angle such that it tightens during deployment. The strands are sewn together at the ends to prevent unraveling. Originally, we were going to use the wheel’s attachment system, but due to time constraints, we cut holes in the Kevlar and bolted it to the stand-in electronics bays.

### 5.2.2 Fill System

The body is inflated through a port that interfaces onto one of the electronics bays. The hermetic layer is attached to the electronics bay via a soft PTFE gasket face seal. A flex hose is connected to the hole and routes around to sit outside of the electronics bay. Figure 9 is a plumbing and integration diagram of the system to explain how the system is filled.

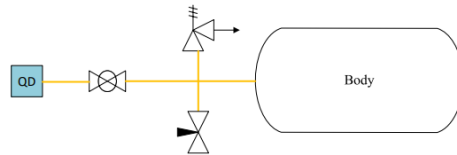


**Figure 9.** Inflatable body plumbing and integration diagram. Pressurant flows through the quick disconnect to the ball valve. It releases pressure via the needle valve and relief valve.

### 5.2.3 Collapsible Rods

Three sets of collapsible rods provide torsional and radial rigidity to the system and mounting points for the cargo bed. We designed the rods to be able to support the expected cargo weights without the supporting inflatable body for safety, but on the moon thinner aluminum or carbon composite tubing could be used in conjunction with the inflatable body. The sets of collapsible rods are set in a triangular shape to maximize the robot's rigidity, minimize displacements from torsion, and allow for the placement of the inflatable body such that it can provide support to the cargo bed.

0.06” Wall Thickness		0.11” Wall Thickness	
Angular Displacement (deg)	Torque (N-m)	Angular Displacement (deg)	Torque (N-m)
0.2	1.20	0.2	2.13
0.45	1.87	0.45	2.93
0.7	2.28	0.7	3.47and

**Table 2.** Twist angles and the corresponding torque required to twist the collapsible rods.

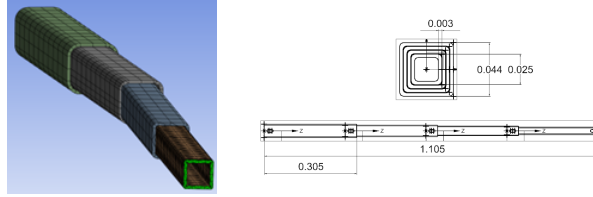


**Figure 10.** Ansys bent CAD model of collapsible rod sections, demonstrating exaggerated deformation of rods due to twist and load

### 5.3 Controls System

The controls prototype is a testbed to ensure interoperability of our electronics, and to gain experience with developing a control system. It was assembled using a 6 inch by 4 ft plank of wood as the body, and 3D printed parts to mount electronics. Ultimately this testbed was upgraded throughout the project and ended up being the final controls prototype.

#### 5.3.1 Electronics

The electronics relevant to the control algorithm are the computer, the inertial measurement unit (IMU), and a pair of brushless electric motors. Our computer is the Nvidia Jetson Orin Nano Developer Kit, a general purpose computer commonly used for robotics because of its integrated Graphics Processing Unit (GPU). The GPU makes it ideal for computer vision and navigation tasks. The Orin interfaces with all hardware onboard, including an IMU for orientation, and a handheld joystick for teleoperation. The data from the IMU and joystick are used as an input to the control algorithm, which computes drive commands based on the robot's state. Figure 11 shows how each input's data is processed in the Orin.

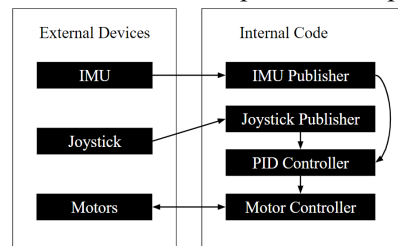


**Figure 11.** Block Diagram, showing the interactions between the external devices and the internal software

Our IMU is the Adafruit BNO085, which has 9 degrees of freedom and open source drivers. It offers orientation reporting, which allows us to read the pitch and yaw of the robot with the built-in sensor fusion algorithm. The IMU communicates over I2C with the Orin and reports orientation data at around 180 Hz. The report rate of orientation data is a critical value for the control algorithm, as it is directly proportional to the response rate of the controller itself.

We selected the T-Motor AK80-9 motor for our final design based on a simulated velocity profile from our requirements. These motors can exert 18 N-m of torque, which is more than sufficient for our system. We calculated that our designed speed of 2.5 m/s the motors would draw a maximum of 7.6 1 A. The motors are rated for 20 A of current, which provides a safety factor of 2.7 when driving. The Orin communicates with the motors through drivers developed by the Open Source Leg[6] project.

#### 5.3.2 Software

The Orin Nano operates using the Ubuntu linux distribution, which is layered with the Robot Operating System (ROS2) to coordinate all software on the robot. ROS2 serves as middleware, collecting and sending data from the various components on the robot for computation. In Figure 11, the links between each device and its software are facilitated by both Ubuntu and ROS2. Due to the complexity of modeling the system in 3D, we opted to model the robot with two planes. In the X-Z plane defined in Figure 12, we implemented a PID (Proportional-Integral-Derivative) control algorithm to manipulate pitch of the central body. In the X-Y plane, we created a separate PID that controls the yaw of the system. These two control

loops are referred to as the lean and turn controllers. PID calculates the difference between a desired value and the current value, and differentials and integrates that error to obtain an estimate of the robot's state. This error calculation is weighted by tuning coefficients and then output as a motor command. By repeating this algorithm at a high refresh rate, the robot will eventually reach its desired control values.

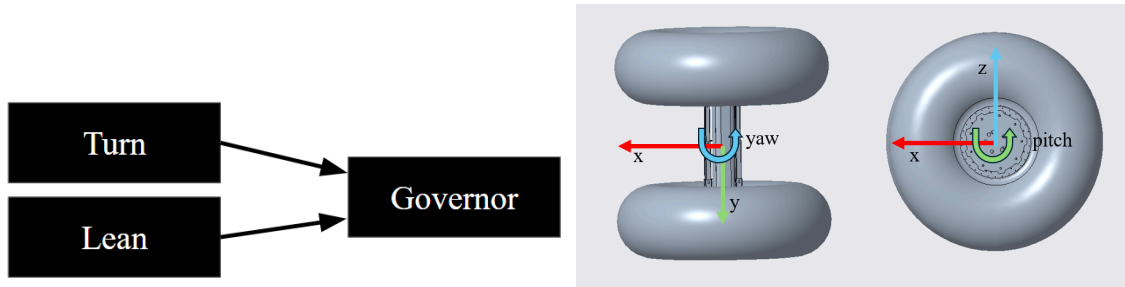


**Figure 12.** (left) PID controller state diagram. (right) Coordinate system for controls prototype.

Due to the planar model of the system, both the lean and turn controllers can come into conflict. By sending conflicting commands to the motors, the system would go into unrecoverable oscillations. To prevent this we use a governor PID controller to manage the final output to the motors. Through the governor, the relative strength and effect of the yaw and pitch commands can be adjusted. The system is tuned to prioritize the lean controller, as it directly controls the balance and linear acceleration of the robot.

A full repository of our code can be found here: <https://github.com/Umich-NASA-Big-Idea-Challenge> .

#### 5.4 Thermal Analysis

A back-of-envelope thermal analysis, as shown in Appendix A, suggests Cargo-BEEP can withstand the lunar environment without dedicated thermal regulation components. The thermal analysis considered the wheel and body subsystems to be decoupled, considered no heat loss from radiation or conduction, and assumed the motors ran at maximum current to provide a worse-case scenario estimation. A basic thermal analysis was performed based on the mission profile, assuming 1.5 hr of driving, 7.5 hr idle, followed by 1.5 hr of driving. The results are summarized in Table 3. The prototype's hermetic layer and electronics would not be able to withstand these temperatures. However, many polymers and films exist in the packaging industry that have low permeability at +200 C. The onboard electronics may experience temperatures upward of 85 C, which could be remedied with thermal insulation to further slow the heat exchange. The wheels have proven operable over a broader pressure range than listed in Table 3. The body can be pressurized to near-rigidity, such that the increased pressure has minimal effect on system function.

Subsystem	Initial pressure (psi)	Final Pressure (psi)	Initial Temperature (C)	Final Temperature (C)
Wheel	20	27	20	117
Body	35	47	20	84

**Table 3.** Results from thermal feasibility analysis of wheel and body subsystems.

#### 5.5 Structural analysis

Structural analyses performed throughout the design and development process informed major design decisions. Finite element analysis (FEA) of the final prototype and concept design suggest that Cargo-BEEP could exceed payload capacity requirements significantly. Kevlar and Vectran are an order of magnitude stronger than steel, and all loads on both the wheel and the body are distributed. This allows us to ignore the complex problem of deformation and stress in the inflated softgoods, as the metal components interfacing with the softgoods would fail first.

The primary rigid load-bearing components of the system are the wheel hub, collapsible rods, motor shafts, and e-bay. The wheel hub experiences an approximately evenly distributed load from the tire pressure and an approximate point load at the center where the shaft of the motor connects to the e-bay. The motor shaft experiences coupled loads from the body and wheel. The body experiences a distributed

load from the cargo. The collapsible rods exist primarily to prevent twist and aid in even deployment. Two structural models were created, one to assess the stresses and deformations experienced by the robot when statically loaded, and one to assess the torsional rigidity provided by the collapsible rod system. Steps necessary to reproduce these analyses are outlined in Appendix B.

The structural analysis of the cargo bed was performed by modeling all structures as being made of 18-8 steel, as was the case for the prototype. Lunar gravity was assumed, and a 20 psi ( $1.38 \times 10^5$  Pa) pressure load was applied to the wheel rims, replicating the inflated wheels. A static stress analysis was performed in Creo, as summarized in Table 4.

Cargo load	Max. Stress	Max. Displacement
300 kg (500 N)	56 MPa, concentrations at standoffs on e-bay and motor shaft	0.5 mm at cargo bed
500 kg (812 N)	120 MPa, concentrations at s standoffs on e-bay and motor shaft	0.8 mm at cargo bed
1000 kg (1625 N)	160 MPa, concentrations over 70 MPa on body, edges around cutouts for rods in e-bay face, standoffs, and motor shaft.	1-2 mm at cargo bed

**Table 4.** Maximum stress and deflections of the cargo bed for various cargo configurations. As the cargo bed is elastic and its stiffness is driven by pressure, the displacements are inaccurate.

Due to the nature of woven inflatable softgoods, the torsion model ignored the inflatable body and considered a system consisting of the wheel hubs, e-bays, and collapsible rods. Opposing moments were applied through each motor shaft at 18 N-m, twice the maximum rated torque for the AK-80 motors used in the prototype. A static structural analysis was performed with the wheel clamped at one rim. The rod segments were connected with the Creo fastener connection. The results are shown in Figure 13. The maximum stress experienced by the rods was 153 MPa, below the yield stress of the materials by 50 MPa. Note that this is a highly conservative estimation and the motors would be unable to sustain such a load without rapidly burning out.

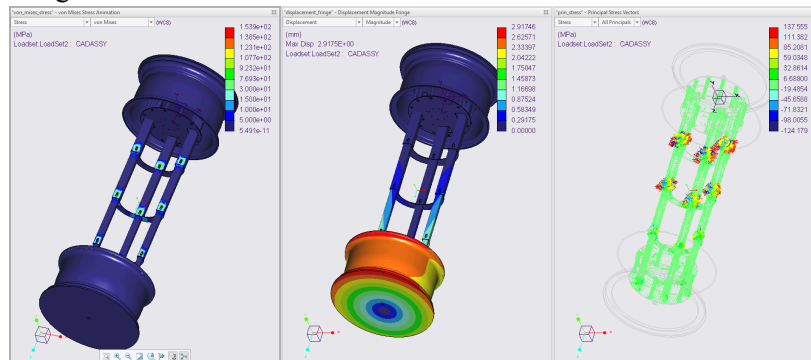


**Figure 13.** Torsion analysis of collapsible rods indicates that torsional stress concentrations at pin slots.

In the absence of a cargo bed, the tolerance between the rods would allow for a greater twist. The gaps between the rods allow for a rotation of approximately  $0.54^\circ$ , which was reduced through the installation of brackets. A single set of rods was simulated due to computational limits, causing the simulation to assume no rotation from slop. Thus, the zero for angular displacement in Table 3 is  $0.54^\circ$ . Differential rotation of the wheels results in up to 9 N-m of torsion on the rods (3 N-m on each set). Driving over an uneven surface while turning produces negligible deflection. Our displacement driven simulation shows less than  $0.7^\circ$  of displacement additional to rod slop at our maximum potential torsion.

### 5.6 Deployment Mechanisms and Operations

To deploy, Cargo-BEEP will be placed in the vertical orientation. The wheels will be inflated first, each wheel individually. A flexible hose will be connected to the quick disconnect on the bottom wheel. The hose will then be pressurized to 30 psi ( $2.07 \times 10^5$  Pa). The ball valve will then be opened, allowing pressure in the wheel to reach 30 psi. The ball valve will then be closed and the flex hose will be depressurized via an upstream vent. The quick disconnect will then be decoupled. This process will repeat on the top wheel. The flex hose will then be attached to the quick disconnect on the body. The same

process will be repeated on the body, extending it to the full deployed height of 1 meter, then allowing the robot to tip over for operation.

### 5.7 Risk Management

ID	Summary	L	C	Trend	Approach	Risk Statement
2	Hermetic Layer	5	5	↑	M,R,W	Hermetic layer fails to hold pressure for duration of use
8	Abrasion Layer	2	3	→	R,M,W	Abrasion layer abrades more rapidly than expected
17	Collapsible Rods	3	3	→	M,R	Failure of locking system for collapsible rods
19	Collapsible Rods	1	3	↓	M,R	Failure to deploy collapsible rods
22	Hermetic Layer	5	5	↑	M,W,R	Hermetic layer seams fail when pressurized
26	Thermal	2	5	↓	M,R	Vacuum conditions cause electrical components to fall out of operating range
27	Software	1	5	→	M,R	Control software reaches an unrecoverable state
28	Electrical	4	1	→	A,W,M	Testing conditions lead to individual component failure
29	Navigation	4	2	→	A	The robot is stuck due to environmental conditions
31	Restraint layer	3	3	NEW	M,W	Restraint layer is moved via friction, resulting in one side of the wheel being less restrained

**Table 5.** Cargo-BEEP’s risk summary. The top ten remaining risks for the project are listed. The L column is for likelihood of the risk occurring. The C column is for the consequences of the risk. In the approach column, M is mitigate, W is watch, R is research, and A is accepted.

Two major risks, 2 and 22, were identified too late to be properly resolved. The initial choice for the hermetic layer, polyurethane coated nylon, would not seal along the seams. We proceeded with our backup, PET, but we encountered the same difficulty during the final stages of manufacturing. While sufficient in small-scale tests, the PET would simply rip along the seam for longer seams. This problem needs to be solved before the body or wheels can be further developed. The mitigation plan would be to identify a new material for this layer. We had other candidates from the initial research on materials, however, we were not able to obtain any on such short notice.

Risks 26, 27, 28, and 29 require the controls prototype or a fully integrated prototype to be subjected to more substantial testing than we were able to complete. The destruction of some hardware being used on the controls prototype is to be expected, as we would be attempting to subject it to harsh conditions to force the control software to reach an unrecoverable state.

Risks 8 and 31 will require a fully manufactured wheel that can be rolled. Once that is complete, we can revisit these risks.

Risks 17 and 19 pertain to the body chassis system. We were unable to properly test the locking system of the collapsible rods. We do foresee it being a risk, with the design potentially needing changes to work. We are confident this can be resolved with time and testing. The failure to deploy rods would occur due to the premature locking of the collapsible rods, likely from friction between the rods. We did not see this occur while we were testing, however, we feel that this is still a risk until further testing has occurred.



## 6.0 Verification Testing on Earth

### 6.1 Wheel Dynamics and Material Usage

Several verification tests were planned to aid in the design of the wheel. Due to time constraints, some were removed or descoped, allowing us to focus on traction testing and material validation.

#### 6.1.1 Traction

The controls prototype was tested in a sandy environment with a low cone index similar to the lunar regolith [7]. We investigated how varying the treads and pressure of the wheels influenced the maximum accelerations, speeds, and motor torques. Our testing setup consisted of a long stretch of flattened sand and a 2 meter long hill at a 12° incline[8]. Each test consisted of the robot driving along a path and then up the hill. We tracked the acceleration of the robot by setting up a camera 100 ft from the path. We used Logger Pro, a data collection and analysis software, to compute the instantaneous acceleration. We performed four tests: a fully-inflated control test with no treads, a partially-inflated control test with no treads, foam treads placed radially every 10°, and foam treads placed radially every 20°. The tread styles we tested can be seen in Figure 14 (left).

The control tests were used to define a baseline of the robot's drivability on lunar regolith. The partially deflated wheels were tested to characterize the impact of a lower pressure on the acceleration of the wheels. This test was motivated by sand racing cars that use deflated wheels to increase the contact patch with the ground and thus increase the amount of draw-bar pull their wheels could generate for a given power (see Figure 14 (right))[9]. The foam tread designs were derived from sand tires, where paddles are used to displace the soil and move the vehicle forward. However, we needed to use symmetrically patterned treads, as the robot is required to be able to move forward and backward to navigate the terrain and turn.

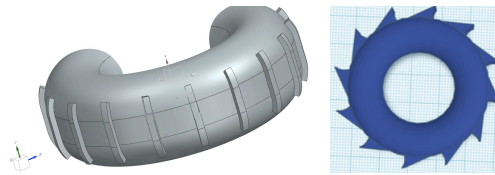


**Figure 14.** (Left) Symmetrical tread design that allows for backwards movement. (Right) Non Symmetrical tread design that does not allow for backwards mobility.

The angular offset of the treads was varied to see if there was a noticeable difference in the amount of acceleration gained from increasing the number of paddles. As seen in Figure 15, both treaded tires and deflated tires had a negative impact on the acceleration performance, so we decided to move forward with the data we had in order to focus on other aspects of the system.

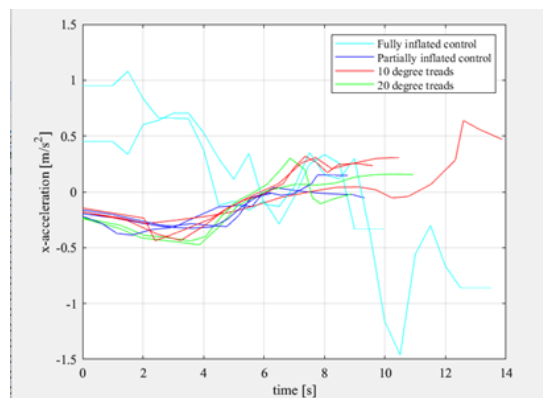


**Figure 15.** Acceleration over time of tested wheels. Partially inflated tires and treaded tires behave similarly.

We initially planned to test two other tread patterns inspired by past lunar rover treads. We also planned to vary tread depth and material. These tests were not completed, because as the control algorithm matured, it became evident that the robot could not produce enough torque to force the wheels to slip in expected terrains.

Traction testing ran into a myriad of challenges. Subproject leadership experienced multiple changes, and the large quantities of treads required for the test were labor intensive to produce. The treads were then difficult to adhere to the controls prototype's polyethylene wheels. There was then a substantial amount of time and personnel required for every test. Finally, the controls algorithm was incomplete at the time of testing.

### 6.1.2 Puncture Testing

Puncture testing was conducted following ASTM F1306-21, the *Standard Test Method for Slow Rate Penetration Resistance of Flexible Barrier Films and Laminates*[10]. A puncture test rig was built according to the specifications of the ASTM standard (Figure 16). Both puncture force and puncture work were measured for 19 commercially available materials following the experimental procedures described in the ASTM standard in an Instron 5585 load frame.



**Figure 16.** The ASTM F1306–21 puncture testing rig mounted in the Instron load frame.

The results are summarized in Figures 17 and 18. Vectran vastly outperformed all other materials, but its susceptibility to UV radiation disqualified it as an abrasion layer. TPU coated UHMWPE (Venom) and 1680D Ballistic Nylon were the second and third contenders respectively for force resistance, with Venom nearly twice as resistant. For total work to puncture, UHMWPE and Ballistic Nylon performed on par with each other. Nylon's extensive history of use as an abrasion-resistant material in the military and aerospace industries made it a more favorable choice.

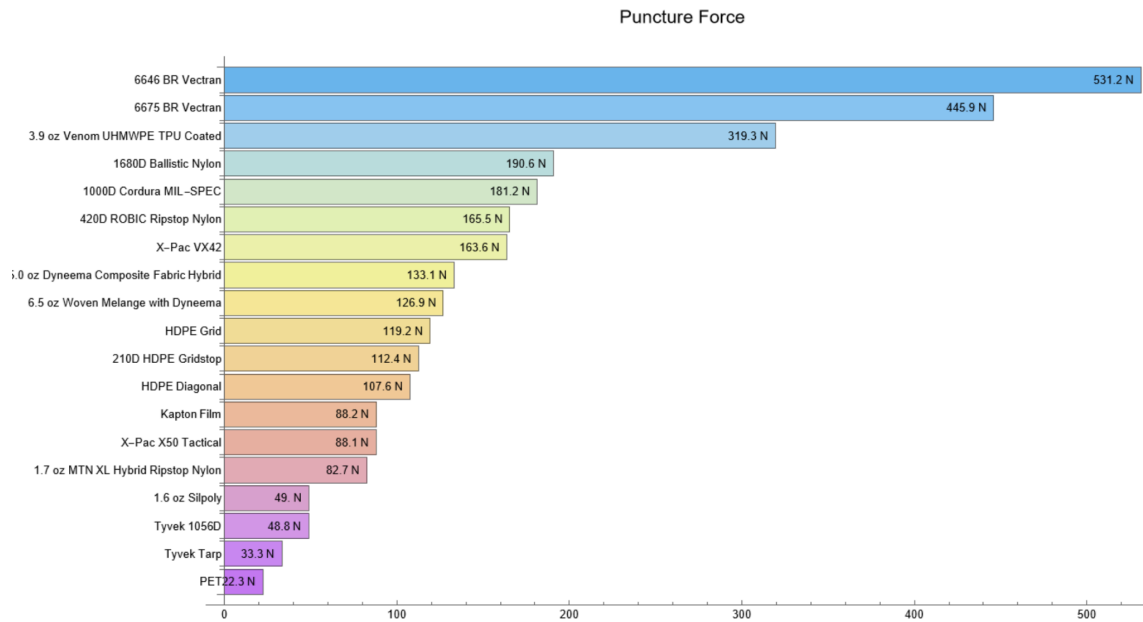


**Figure 17.** Peak puncture force before mechanical failure, calculated using the procedure in ASTM F1306-21.

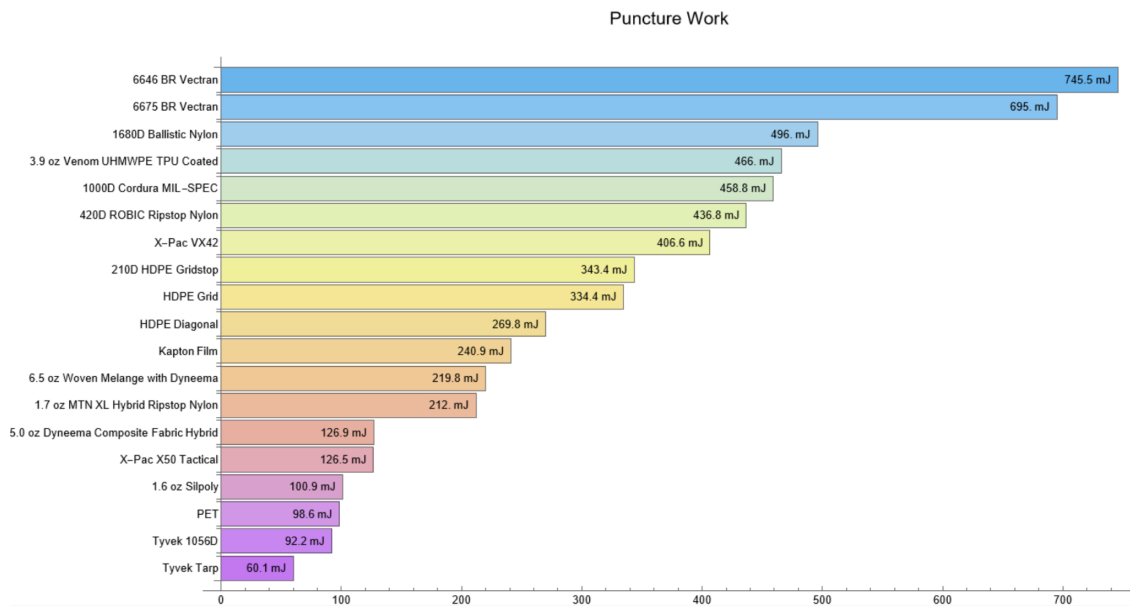


**Figure 18.** Peak puncture work before mechanical failure, calculated using the procedure in ASTM F1306-21.

To make the final selection, UHMWPE and Ballistic Nylon were stress tested with Kevlar scissors, a pocket knife, sanded with a file, and heated with an impulse sealer (Figure 19). Both materials showed excellent resistance to slashing. Ballistic Nylon slightly outperformed UHMWPE in resistance to abrasion. When exposed to an impulse sealer, UHMWPE lost its integrity and became brittle, easily tearing, while Ballistic Nylon sustained minimal damage. Therefore Ballistic Nylon was chosen as a more robust choice.

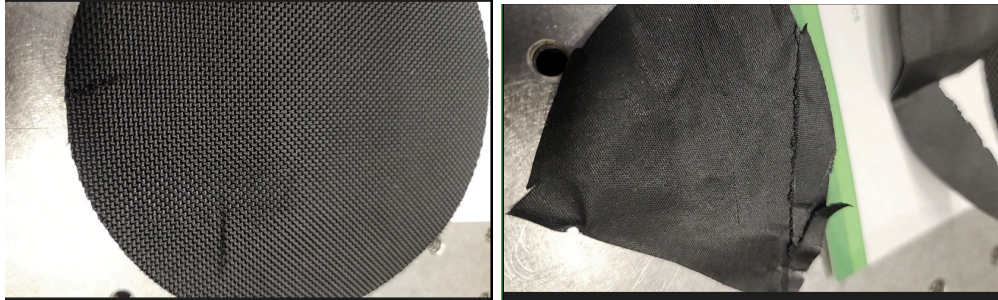


**Figure 19.** (left) Slash testing of Ballistic Nylon with an X-Acto knife and Kevlar scissors. (right). UHMWPE heat seals tore with minimal effort.

## 6.2 Body Deployment Testing

Prior to the mid-project report, we tested the feasibility of the deployable chassis with a simple small-scale prototype. We wanted the next step to be full-scale integration of all inflatable components, with wheels and deployable chassis systems on the same rig. However, due to time constraints, we tested the inflation of the body and the wheel separately. To accomplish this task, we constructed a full-scale deployment rig that demonstrates the primary deployment mechanism (Figure 20). This rig contains a simplified version of the body’s fill system, full-scale collapsible rods, and a prototype inflatable body. The rig fully deployed, but it only survived two inflation cycles before the seam of the hermetic layer failed and began to leak.



**Figure 20.** Primary deployment rig

## 6.3 Controls System

### 6.3.1 PID Tuning

Verifying the efficacy of the control system was a time consuming and resource intensive process. The algorithm had to maintain the desired lean and turn of the robot while resisting disturbances from terrain. Meeting this goal required hours of tuning, data collection, analysis, and re-tuning. Over the course of development, the system matured from maintaining stability only on indoor surfaces to taking harsh outdoors terrain.

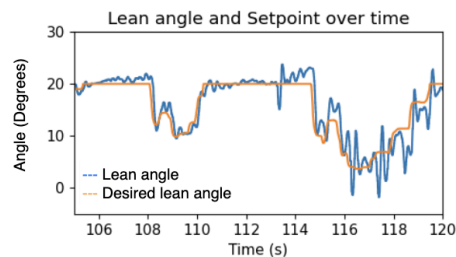


**Figure 21.** Controller setpoint and true angle of body over time. The desired lean angle is the setpoint. To analyze how the system reacts, we graphed the inputs and outputs of the system over time. Figure 21 shows data from a snapshot of a trial run. It displays the response of the system against changes to the desired lean angle. Using this method, we were able to tune the lean controller to be responsive to changes in setpoints and disturbances. For the turning controller, we prioritized a smooth and responsive feel for the human operator, using qualitative observation to optimize it.

### 6.3.2 Wave Field Testing



**Figure 22.** University of Michigan Wave Field[11]

The controls prototype was stress tested on the University of Michigan Wave Field, shown in Figure 22. The hills have a grade of approximately  $45^\circ$ . The 75th percentile grade on the moon is  $12^\circ$ [8]. This test was meant to be an extreme simulation of the system driving over craterous terrain. The robot could not drive through the entire Wave Field, but could clear several hills on each attempt. This is because of the geometry of Segway-style robots. The maximum acceleration the robot can output while maintaining balance is a function of the mass of its pendulum. As a result, the controls prototype is too light to climb up the hills without building momentum first.

### 6.3.3 Controls Prototype Safety Considerations

The controls prototype operates with high torque and uses lithium-ion batteries, both of which have the potential to harm personnel. Working with high-power systems poses the risk of short circuits and overcurrents. In order to mitigate these risks, we employed software and hardware safety protocols.

We programmed a software shutoff, which commands the velocity of the motors to zero and ends the process that controls the motors. It can be triggered by the human operator using a button on the joystick. This method is preferred, as it does not cut power to the motors, which halts communication with the Orin. However, the software stop requires a wireless connection to the robot. To establish wireless connection, we employed the Secure Shell (SSH) protocol to access and run commands on the robot from another computer. The range of wireless connections to the robot are limited to the range of the WiFi antenna onboard.

Hardware shutdowns were installed to ensure that the robot could be stopped when out of range. The first hardware stop is a relay box wired into the power supply of the motor that operates via radio. It can be triggered remotely at a much greater range than the software shutdowns. Additionally, there is an emergency stop button on the robot that breaks the circuit made by the batteries, killing power to every component on board.

During outdoor testing, a minimum of three people were required to be present to ensure the robot could be handled safely. One person would drive the robot with the joystick controller, another would manage the software via laptop, and the third would observe the robot.

### 6.4 Thermal Vacuum Testing

Initially, Cargo-BEEP was to undergo subsystem level testing in a small thermal vacuum (TVAC) chamber and system level testing in a large vacuum chamber. We had reached out to two separate laboratories at the University of Michigan to use their testing facilities during the proposal phase. Both facilities had windows we could utilize between September and early October, but requested we reach out in August to confirm the window. After reaching out in August, we learned that the large vacuum chamber booked another test during our window. We then proceeded to plan on using the smaller vacuum chamber for more in depth subsystem tests, using the allocated budget for the larger chamber for extra time in the small chamber.

The subsystems were incompatible with the smaller chamber due to the original intent of using the larger chamber, requiring the team to pivot and make significant design changes. This, among other manufacturing difficulties, resulted in the decision to utilize COTS wheel rims. The COTS wheel rims required the system to be redesigned, resulting in significant delays. Due to the wheels being considered a critical path, the inflatable body and collapsible rods were not prioritized, resulting in schedule slips. On

September 30th, team leadership saw that neither subsystem would be prepared to go into vacuum within 7 days, and made the decision to cut TVAC testing.

## **7.0 Path to Flight**

The flight wheel rim would be a 40 cm open-faced cylinder cast out of stainless steel. It would have 4 inch flanges for the gasket. The gasket would be a 40 cm ePTFE gasket, sized and compressed according to the FSA[12]. A secondary lining of RSV silicone or suitable adhesive for the hermetic layer would act as a secondary seal to prevent catastrophic decompression in the event of gasket failure and reduce permeation of gas.

A new hermetic layer material would need to be selected. Coated Nylon has flight history, but our team lacked the ability to effectively seal it with available technology. Packaging films such as Cepak and Combitherm have also been explored in inflatable habitat studies and have permeabilities lower than Nylon by orders of magnitude[13][14]. For the restraint layer, Vectran would be used instead of Kevlar to reduce creep over the mission span, and radial straps would be included to decrease the load on the hermetic layer.

A wider range of treads and pressure tests would be conducted according to the originally proposed traction testing plan. Semi-rigid hinge patterns may be incorporated into the wheel to aid in structured collapse and inflation and provide a better shape than a pure torus.

Argon is preferred to fill inflatable systems due to its thermal stability and reduced permeation compared to lighter stable gasses. N<sub>2</sub> may be an acceptable compromise due to its lower cost and higher availability.

The inflatable body can be improved for flight by adding a semi-rigid collapsible insert, providing a structured collapse and a flatter body for the cargo bed. The cargo bed would be designed with a quick catch-and-release system involving clips and pins for easy attachment post-deployment. We would also incorporate a kickstand to the chassis for when the vehicle is not in use in the inflated state.

The collapsing rods would need a self-locking mechanism once fully deployed to prevent sliding and to increase torsional rigidity. The locking mechanism could consist of spring-loaded locking pins at each rod-rod interface, with the pins being engaged and disengaged with a mechanical button on the rover. The engagement and locking mechanism could be similar to the mechanism used in the collapsing rods of suitcase handles.

Cargo-BEEP requires several electronic and controls changes for flight. The rover requires temperature and pressure sensors to monitor its condition. Additionally, an RGB-Depth (RGBD) camera would need to be installed and mounted to allow for local navigation. The rover would need to communicate via radio instead of WiFi. The emergency stop protocols would be improved to ensure the rover can operate safely.

Cargo-BEEP has very few delicate or brittle components, and substantial built-in cushioning from the softgoods components. It would be straightforward to fill empty spaces surrounding electronics with lightweight shock-absorbing foam. This could make it feasible for Cargo-BEEP to be dropped from an orbiting or flyby vehicle and perform an airbag landing. Alternatively, Cargo-BEEP could be included on a landing vehicle. Since the design can be manipulated with minimum effort and does not have a ‘correct’ orientation in compact form, minimal controls would be needed for this drop, and care would only need to be taken to ensure it lands within reach of astronauts.

## **7.1 Path to implementation**

### **7.1.1 Wheels**

We have an inflatable prototype that can inflate and deflate. Our path towards flight would include designing a hermetic layer of a more suitable material and resizing it to 1.5 m. A second wheel would be built based on lessons learned and the original wheel would be adjusted to match specifications. We currently possess the shaft-hub adapter plates that can be integrated with minor modification. We would machine the axle in such a way that it would prevent the wheel from sliding off via adaptations to the shaft hub.

### **7.1.2 Body**

Our testing demonstrates the feasibility of the deployment system. The initial deployment prototype would be further validated by completing implementation of our planned design. We would integrate with

the wheels to validate our integrated system. Furthermore, the rods cross-section will be changed to circular to mitigate binding. We would complete our current cargo bed design and install it to have a configuration that can be fully tested in TVAC to validate our system in a lunar thermal environment.

### **7.1.3 Controls System**

Testing of the controls prototype demonstrated that the physical system is controllable and meets the requirements that we have set. A more sophisticated control algorithm would require accurate linear velocity data, which our current electronics cannot deliver. We would purchase a higher quality IMU and implement a data filtering algorithm such as the Kalman filter. Signal lights would be integrated to communicate the robot's operational status, motion, and condition.

## **7.2 Continued Development**

With the remaining funds, we plan to proceed with final integration. Currently, we are close to having a fully integrated prototype.

### **7.2.1 Wheels**

The wheels have been used to determine softgood materials. We would like to put our choices through more rigorous testing, including TVAC, burst, and creep testing. We would continue exploring wheel dynamics parameters, such as tread types, in the case that the inflatable wheel design is beneficial for stakeholders. We would develop more reliable and repeatable methods of manufacturing the wheels, particularly the hermetic layer.

### **7.2.2 Deployable Chassis System**

The inflatable body suffered from sizing and manufacturing challenges, as it was undersized and improperly sealed; we would design a rig for the manufacturing and sealing of the hermetic layer. The collapsible rods suffered from binding issues and lacked a built-in locking mechanism; we would redesign them to be circular and have a locking mechanism. The slots in the collapsible rods would be padded with foam to reduce noise, and they would be resized for the final design. The chassis as a whole would require multiple cargo bed arrangements. Initial ideas include surface sample and hand tool storage. After the deployable chassis system is manufactured, we would perform cycling deployment tests. We would test deployment in a sandy environment to identify dust ingress risks and implement solutions.

### **7.2.3 Controls**

We plan to continue development on the controls with a fully integrated system, potentially using a torque-based velocity controller due to the increased mass of the wheels. We have purchased an RGBD camera to use for autonomous navigation. Additionally, we plan on using simulations to test the control algorithm in lunar environments. The Robot Operating System (ROS2) has a companion simulation software, Gazebo, which has allowed us to run simple simulations. We need to further understand the software before we can begin simulating the robot on lunar terrain.



## **8.0 Project Management**

### **8.1 Leadership**

Team leadership changed twice, following the availability of people able to lead. Shai Toledano and Raven St. Clair served as co-leads until the summer and then transferred leadership to Jason Brown and Michael Robinson. This first leadership transition was difficult, since both previous leads left directly after the semester ended. The second leadership transition involved Jason Brown handing over his role to Hannah Cherry, which was a much smoother process because of better communication and the continuity of one lead.

Phase 1 leadership focused on the research and design of Cargo-BEEP, and established three subteams that worked to develop initial prototypes for the primary subsystems. The availability of volunteer labor over the summer decreased due to most members leaving the state for summer break. The team determined that there was sufficient funding to hire two full-time workers and one part-time worker, with the full-time positions allocated to Jason Brown and Michael Robinson and the part-time position allocated to Christopher Packard. Funding was allocated to those with the most availability and who expressed that they would not be able to work in their fullest capacity otherwise. Most members continued work over the summer as volunteers.

Due to the lack of personnel over the summer, leadership in this period was more focused on technical development, which resulted in administrative tasks slipping. A few weeks prior to the mid-project report deadline, Hannah Cherry stepped in and took leadership of many administrative tasks. During this period, major design decisions were often reserved for all-hands meetings with both in-person and virtual members. While important to team adhesion, this hindered rapid iteration from in-person members. In hindsight, more autonomy should likely have been granted to individual subteams and in-person members.

After summer break, feedback from team members saw the team's leadership and management style become more collaborative. With the majority of team members working in person, issues and changes were discussed more rapidly and progress accelerated. As the team's efforts shifted to manufacturing, our faculty advisor, Professor John Shaw, became more involved in the decision making process.

Throughout the project, Cargo-BEEP used the messaging platform Discord to communicate. We initially used it during the proposal phase, as it was easier for the initial team members to communicate through it. We used Google Drive as our primary file management platform. The controls software was managed via Github and CAD was stored in Siemens TeamCenter. We chose these platforms due to having access through the University of Michigan and much of the team having prior experience navigating them.

Each subteam had one formal general meeting per week, in addition to worksessions, discussions, and impromptu meetings. The team as a whole had one all-hands meeting per week, which was used for important announcements, updates, and asking questions.

### **8.2 Schedule**

Our schedule underwent significant changes between the proposal and mid-project report. As such, we will discuss our mid-project report schedule and how it changed throughout Phase 2 of funding.

#### **8.2.1 Mid-Project Report Schedule**

##### March-April:

- Recruitment of team members to expand team capabilities.
- Formation of three subteams and assignment of team members based on skill sets: materials, deployment mechanisms, and driving prototype.

##### April-May:

- Established preliminary softgood materials and basic testing parameters; initiated research on folding methods and optimization.
- Corrected design for burst test pressure hubs, ordered necessary materials, and manufactured an extended version of the collapsible rod mechanism.

- Created Simulink model to test a linear-quadratic regulator for controls prototype balancing.

#### May-June:

- Designed a full traction testing rig.
- Transitioned to resin printing for prototyping.
- Selected the electronics required for the controls prototype.

#### June-July:

- Weave samples of Vectran for testing and started inflating a wheel mockup.
- Run thermal analyses of the gas in the wheels and deployable chassis system.
- Begin design for a collapsible cargo bed.
- Build the physical controls prototype and demonstrated balancing capabilities.
- Perform gas permeation testing for bladder layer, weave design for restraining layer, preliminary thermal testing.

#### July-August:

- Conduct transverse loading tests on the collapsible mechanism and test collapsible bed under load.
- Perform full-scale traction testing and finish material testing.
- Test electronics and software with simulated test data, testing of potential edge cases, and failure modes. Test UV radiation-proofing and thermal insulating housing.
- Ensure the robot prototype can be driven around and test it in a simulated lunar environment.
- Perform material abrasion, corrosion, and puncture testing.

#### August-September:

- Manufacture the final prototype.
- Run thermal and vacuum testing of electronics and pneumatics.
- Perform creep testing, burst testing, lifetime and fatigue testing.
- System-level integration.

#### September-October:

- Testing of advanced prototype in earth environment, including pressurization, deployment, and locomotion.
- Verification of loads, stress, and temperature requirements.
- Testing of autonomous and controlled navigation systems on the final model..

#### October-November:

- Full scale testing in large UM Plasmadynamic and Electric Propulsion Laboratory (PEPL) vacuum chamber.
- Report preparation and next steps.

### **8.2.2 Schedule Changes**

Throughout Phase 2, some of the smaller items on the schedule began to slip or were cut to ensure there would be time to fully test and integrate Cargo-BEEP. Creep, burst, lifetime, and fatigue testing were cut due to lack of resources.

The amount of resources required for traction testing was greater than we had anticipated. We began prepping early August, but were unable to test until mid-September. As mentioned in section 6.4, Cargo-BEEP was unable to enter TVAC due to design changes required to fully test subsystems in a smaller vacuum chamber. As such, the final two months of our schedule pertaining to final prototype testing and integration slipped substantially. Due to unexpected manufacturing challenges with the initial wheel and deployable chassis, we reached the end of September without hardware ready for TVAC.

We did not have time to manufacture two wheels, integrate, and test the entire Cargo-BEEP system. After consulting with NASA, we came to the decision that we would attempt to place a wheel and the deployable chassis in TVAC and demonstrate controls via the prototype. Due to the challenges with the hermetic layer, we were still unable to enter TVAC.

### 8.2.3 Schedule Difficulties

One of the major schedule challenges we saw throughout our project was understanding what materials we should be using for the fabric layers of the inflatables. We reached out to multiple companies to request samples and consultations, but most responded by saying they were either not able or not willing to work with us. We then had difficulties with obtaining samples/materials from available suppliers, with multiple packages getting lost by the postal service. As such, it took us significantly longer to both select the materials and obtain them to begin prototyping.

### 8.3 Budget

Description	Phase 1 2/1/24 - 6/30/24	Phase 1 Spending	Phase 1 Remaining	Phase 2 7/1/24-12/31/24	Phase 2 Total Starting	Phase 2 Spending	Phase 2 Remaining	Total Allocated
<b>A. Direct Labor - Key Personnel</b>	\$ -							\$-
Direct Labor - Other Personnel	\$12,900.00	\$21,600.00	-\$8,700.00	\$0.00				\$21,600.00
<b>B. Fringe Benefits</b>	\$986.85	\$1,652.40	-\$665.55	\$0.00				\$1,652.40
<b>Total Labor Costs (A+B)</b>	<b>\$13,886.85</b>	<b>\$23,252.40</b>	<b>-\$9,365.55</b>	<b>\$0.00</b>				<b>\$23,252.40</b>
<b>C. Direct Costs - Equipment</b>	\$ -			\$ -				\$-
<b>D. Direct Costs - Domestic Travel</b>	\$ -			\$16,909.45	\$16,909.45	\$18,971.42	-\$2,061.97	\$18,971.42
<b>E. Other Direct Costs</b>								
Materials and Supplies	\$13,945.00	\$3,901.77	\$10,043.23	\$10,753.30	\$20,796.53	\$15,657.92	\$5,138.61	\$24,706.16
Testing Costs or Facilities Rental	\$ -			\$7,500	\$7,500.00	\$2,470.64	\$5,029.36	\$7,500
Consultants	\$ -							
Services	\$13,350.00	\$0.00	\$3,984.45	\$6,015.55	\$10,000.00	\$816.00	\$9,184.00	\$7,938.04
Subcontracts/Subawards	\$ -							
Miscellaneous	\$ -							
<b>Total Other Direct Costs (E)</b>	<b>\$27,295.00</b>	<b>\$3,901.77</b>	<b>\$14,027.68</b>	<b>\$24,276.71</b>	<b>\$38,296.53</b>	<b>\$18,944.56</b>	<b>\$19,351.97</b>	<b>\$42,206.16</b>
<b>F. Total Direct Costs (A+B+C+D+E)</b>	<b>\$41,181.85</b>	<b>\$27,154.17</b>	<b>\$4,662.13</b>	<b>\$41,178.30</b>	<b>\$55,205.98</b>	<b>\$37,915.98</b>	<b>\$17,290.01</b>	<b>\$82,368.01</b>
Modified Total Direct Costs, if applicable	\$41,181.85	\$27,154.17	\$4,662.13	\$41,178.30	\$55,205.98	\$37,915.98	\$17,290.01	\$82,368.01
<b>G. Total Indirect Costs</b>	<b>\$8,812.92</b>	<b>\$8,812.92</b>	<b>\$0.00</b>	<b>\$8,812.16</b>	<b>\$8,812.16</b>	<b>\$8,812.16</b>	<b>\$0.00</b>	<b>\$17,626.75</b>
<b>H. Total Direct and Indirect Costs (F+G)</b>	<b>\$49,994.77</b>	<b>\$35,967.09</b>	<b>\$14,027.68</b>	<b>\$49,990.46</b>	<b>\$64,018.14</b>	<b>\$46,728.14</b>	<b>\$17,290.01</b>	<b>\$99,994.76</b>
<i>% of Total Budget</i>	<i>50.00%</i>			<i>50.00%</i>				<i>100.00%</i>

**Table 6.** Cargo-BEEP’s budget throughout the NASA Big Idea Challenge.

Cargo-BEEP is under budget (Table 6) due to the decision to manufacture softgoods in-house and to cut TVAC. We operated under the assumption we would need to outsource softgood manufacturing. Because we were unable to work with companies, this portion of the budget was unused.

Due to having a team size larger than anticipated, our initial travel budget to attend the conference was not sufficient. We went \$2,061.97 over budget, which we were able to pull from the services category.

When the team had large purchases, such as the softgood materials and the electric motors, the team would justify it with in-depth research. We tested samples of materials before proceeding to purchasing and we simulated motor performance prior to purchasing. Once we were satisfied with the results, we moved ahead to purchasing.

The team did not receive any sponsorships or sources of funding besides NASA.

# Appendix A: Conservative Thermal Analysis

October 16, 2024

A back-of-envelope thermal feasibility analysis was performed on the body and wheel subsystems of Cargo-BEEP. The analysis assumed heat was added to the system from radiation and electronics only, ignored heat loss from radiation, and assumed the wheel and body were decoupled and did not affect each other. The results were calculated with a safety factor of 1.5 assuming lunar illuminated conditions over the course of a standard mission. The results of the analysis are shown in Table B.1. Assuming ambient conditions of 20 C before mission start, our design can tolerate lunar thermal conditions with the materials specified in the path-to-flight section of this report.

THERMAL FEASIBILITY RESULTS

---

System	$\Delta T$ (K)	$\Delta P$ (psi)
Wheel	65	7.0
Wheel	64	12.2

---

## 1 Mission

A mission is defined as 1 hour of driving, 5 hours of idle, and 1 hour of driving. This corresponds to traveling from the furthest base to the furthest mining site, idling for 5 hours while astronauts work, and then driving back, assuming a 5 mph average speed.

## 2 Assumptions

The following assumptions were made in this analysis

- No conductive or convective heat transfer between the lunar environment and the vehicle.
- Constant illumination
- The vehicle begins the mission at 20 C.
- No gas loss or frictional heating
- All internal heat comes from electronics
- No volume change in wheels
- No radiative heat loss
- Instantaneous heat transfer between all components. Note that more sensitive components (e.g. electronics and the hermetic layer) are the most internal in the system, so this estimate is conservative.

### 3 Theory

The configuration of the materials and lack of availability of thermal conductivity information for some make a theoretical calculation very limited in accuracy. For a preliminary thermal analysis using the assumptions above, a conservative estimate of the temperature change can be calculated as

$$\dot{Q} = mc \frac{dT}{dt} \tag{1}$$

For a basic lumped analysis for all components in a subsystem, the overall temperature change is thus

$$dT = \frac{\sum \dot{Q}}{\sum mc} dt \tag{2}$$

### 4 Thermal Output of Components

Heat estimations were done under the worst-case assumptions that all power dissipated converted into heat and the motors consistently ran at a maximum continuous current of 10.3A. For all electronics excluding motors, we used the provided efficiency ratings and estimated 18.6W of heat from the DC converter and Orin Nano, considering the rest of the electronics produced negligible heat. For the motors, we calculated active (10.3A) and idle (1.25A) power dissipation using an analytical graph of motor operation for efficiency ratings, and arrived at 60W of heat during idle operation and 247W of heat during active operation.

### 5 Thermal & Power Calculations for Electronics

The primary electronic components of Cargo-BEEP are summarized in Table 1.

Electrical Component	Quantity	Power (W)
NVIDIA Jetson Orin Nano	1	6
48-12V converter	1	12.6
IMU	1	negligible
R-link	2	negligible
AK80-9 Motor (Active)	2	123.6
AK80-9 Motor (Idle)	2	60

Table 1: Electronics and nominal power output

#### 5.1 AK 80-9 Motor Specifications

Specifications:

- Operating Voltage: 48V
- Rated Torque: 9N-m
- Rated Current: 10.3A
- Efficiency at 10.3A: 75%

The AK80-9 Motors can safely handle a maximum of 10.3A of continuous current and this value will be used to represent their average current draw during the robot’s movement through rough terrain.

## 5.2 Heat Dissipation During Active Operation

Using  $P = IV$ , we can calculate the input power of the motors. Then, taking the efficiency value of 75%, we can calculate the output power and therefore the total power dissipated.

$$P_{in} = 10.3 \cdot 48 = 494.4W \quad (3)$$

$$P_{out} = 494.4 \cdot .75 = 370.8W \quad (4)$$

$$P_{dissipated} = P_{in} - P_{out} = 123.6W \text{ per motor.} \quad (5)$$

As a worst-case scenario, we'll assume all power dissipated is lost to heat. Taking into account two motors, that leaves us with an estimate of approximately 247W of heat coming from the motors during active operation.

## 5.3 Idle And Peak Operation

Idle Specifications:

- Idle Current: 1.25 A
- Idle Torque: 0 N-m
- Idle Heat Dissipation: 120 W
- Efficiency: 0 %

Peak Specifications (evaluated for a single motor during a momentary spike in power consumption):

- Peak Current: 22 A
- Peak Torque: 18 N-m
- Peak Heat Dissipation: 845 W
- Efficiency: 60 %

Considering two motors:

Idle Heat Dissipation: 120W

Peak Heat Dissipation: 845W

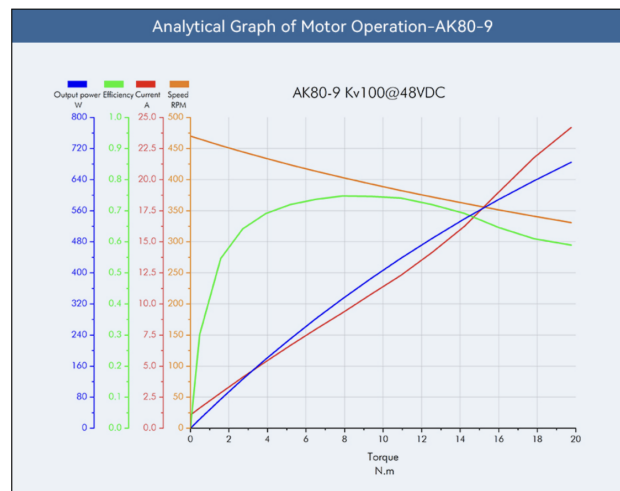


Figure 1: Analytical Graph of AK80-9 Operation

## 5.4 Battery Capacity

The battery capacity formula in A-h is:

$$TotalCurrent = (I_{active} \times T_{active} + I_{idle} \times T_{idle}) \times 2 \quad (6)$$

Scenario 1: Active for 2 hours, idle for 6 (10 mile round trip)  $(10.3 * 2 + 1.25 * 6) * 2 = 56.2$  Ah

Scenario 2: Active for 4, idle for 6 (20 mile round trip)  $(10.3 * 4 + 1.25 * 6) * 2 = 97.4$  Ah

Source [1] <https://www.cubemars.com/goods-982-AK80-9.html>

\*Note: 10.3A value is probably an overkill and could likely change, reducing power dissipation and battery capacity requirement

## 5.5 Other Components

:

### **NVIDIA Jetson Orin Nano**

Input Power: 15W

No efficiency rating specification, so therefore a worst-case assumption would be 15W power dissipation. However, a conservative estimate could be 60% efficiency, and therefore we have 6W of heat dissipation.

Source: NVIDIA Forum Moderator

<https://forums.developer.nvidia.com/t/battery-power-for-jetson-orin-nano/282067>

### **48-12V converter**

Output Power: 240W

Efficiency: 95%

Power Dissipation: 12.6 W

Source: Their Amazon page

[https://www.amazon.com/dp/B0756T983Q?\\_cm\\_sw\\_r\\_cp\\_ud\\_ct\\_9PWZEJOVSH031WE5YFRF&th=1](https://www.amazon.com/dp/B0756T983Q?_cm_sw_r_cp_ud_ct_9PWZEJOVSH031WE5YFRF&th=1)

### **IMU BNO085**

There is no datasheet provided, but a 5mA current draw can be estimated for these kinds of small sensors. With 3.3V and 5mA, it has a 0.0165 power input. For such low powered devices, efficiency tends to be quite high, so therefore heat dissipation can be considered negligible in this instance.

Product link

<https://www.adafruit.com/product/4754>

### **R-Link**

Power Input: > 30 mW

Similar to the IMU, efficiency for low power devices tends to be high, so therefore heat dissipation can be considered negligible in this instance as well.

Source:

<https://www.cubemars.com/images/file/20220307/1646619452473352.pdf>

## 6 Thermal Analysis of Wheel

The wheel was considered to be a torus with an central radius of .4065 m and a tube radius of .2035 m, representative of the prototype wheel. This tire is pressed flush against a wheel rim, approximated as a hollow cylinder with one open face and a diameter of .406 and a height of .2 m. The wheel rim was assumed to be composed of 18-8 stainless steel. Aluminum could also be suitable, steel was the material most readily available to our team for our prototype. The wheel was assumed to have thre thin layers, a hermetic layer made of PET, a restraint of kevlar, and an abrasive layer of ballistic nylon. Note that PET would not be used in a flight version and was chosen as a representative thin bladder material, and vectran would replace the Kevlar. The wheel was assumed to be presurized with Argon to 20 psi. The material properties of these are summarized below:

$$C_{PET} = 1250 \frac{J}{kg - K} \quad (7)$$

$$C_{KEVLAR} = 1420 \frac{J}{kg - K} \quad (8)$$

$$C_{680D\_B\_NYLON} = 1720 \frac{J}{kg - K} \quad (9)$$

$$C_{SS18-8} = 896 \frac{J}{kg - K} \quad (10)$$

$$C_{ARGON} = 523 \frac{J}{kg - K} \quad (11)$$

$$RHO_{PET} = 70 \frac{kg}{m^3} \quad (12)$$

$$RHO_{KEVLAR} = 1075 \frac{kg}{m^3} \quad (13)$$

$$RHO_{1680D\_B\_NYLON} = 110 \frac{kg}{m^3} \quad (14)$$

$$RHO_{SS18-8} = 2700 \frac{kg}{m^3} \quad (15)$$

$$EPSI_{SS18-8} = .04 \quad (16)$$

$$EPSI_{DEFAULT} = 0.1 \quad (17)$$

Where C is specific heat, RHO is density, and EPSI is emissivity

The mass was calculated for each by multiplying their densities by their volumes. The wheel was assumed to be made of three tori of the above material, each 1.5 mm thick. The mass of argon was calculated using the ideal gas law at 20 C. Assuming solar radiation of  $1370 \text{ Wm}^{-2}$  for 10.5 hours (7 hours  $\times$  1.5) over the projected surface facing the sky, the temperature change was 97 K and the pressure change in the wheel was 6.56 psi. See code at the end of this document to reproduce these values.



## 7 Thermal Analysis of Body

The body was considered to be composed of two e-bays, three telescoping rod sets, and the inflated beam. The heat sources were assumed to be radiation from the sun on the inflated beam (the e-bays are obscured by the wheels and the telescoping rods are shaded by the beam) and the heat from the motors.

The e-bay was assumed to be a .35 m diameter hollow closed face cylinder with a depth of .10 m. The rods were approximated as 3 hollow beam square beams with a width of 3.175 cm, a length of 1.2 m and a thickness of 2.74 mm. The inflated beam was assumed to consist of three hollow open faced cylinders of PET, kevlar, and ballistic nylon, with diameters of .1778 m and a length of 1 m. The e-bay and rods were assumed to be made of stainless steel. The body was assumed to be pressurized to 35 psi with argon

The analysis assumed 10.5 hours of sunlight, with 3 hours of motors heat (850 W), and 7.5 hours of idle electronics heat (60 W). The result was a temperature increase of 64 C and a pressure increase of 11.6 psi

## 8 Code

```
import numpy as np

# ALL UNITS METRIC

# MISSION SCENARIO:
# 1 HR DRIVING AT 5 MPH, 5 HOURS AT REST, 1 HR DRIVING AT 5 MPH BACK
# CORRESPONDS TO ROUND TRIP FROM FURTHEST BASE TO MINING SITE
# + CALCULATE TEMPERATURE DROP WITH TIME IN IDLE SHADOW IN CASE OF ACCIDENTAL EXPOSURE

# ASSUMPTIONS
# 1. NO HEAT TRNSFR BETWEEN REGOLITH AND ROVER
# 2. ALL WHEEL LAYERS ARE OF EQUAL SURFACE AREA
# 3. ALL FABRICS 1.5 MM THICK

Q_SUN = 1370
T_0 = 293.15
MOL_MASS_ARGON = 0.4

r = (1.22-.406)/4
R = 0.406/2+r
A_WHEEL = 4* np.pi**2*r*R
A_HUB = np.pi * .406 * .2 + np.pi * .203**2
V_WHEEL = 2*np.pi**2 * R*r**2
T_FABRIC = 0.0015
T_HUB = .005

KAPPA_PET = 0.24 # [1]
KAPPA_KEVLAR = 0.04 # [2], note no data available for specific grade used
KAPPA_1680D_B_NYLON = 1.06 # [3], note no data available for specific grade used
KAPPA_6061T6 = 167 # [4]

C_PET = 1250
C_KEVLAR = 1420 # 170 yds 1" material was used of 1 oz/yd. This density was calculated to work with the
C_1680D_B_NYLON = 1720
C_6061T6 = 896
```

```

C_ARGON = 523

RHO_PET = 70
RHO_KEVLAR = 1075
RHO_1680D_B_NYLON = 1170
RHO_6061T6 = 2700
EPSI_6061T6 = .04

Q_MOTOR_RUNNING = 850
Q_MOTOR_IDLE = 60

epsi_default = 0.1
class Component:
    def __init__(self, A: float, t: float, kappa: float, C: float, rho:float, epsi: float = 0.1):
        self.A = A
        self.t = t
        self.V = A*t
        self.kappa = kappa
        self.C = C
        self.epsi = epsi
        self.rho = rho
        self.m = self.rho * self.V
    def Q_dot(self, q):
        return q * self.A * self.epsi
    def mc(self):
        return self.m*self.C

hermetic_layer = Component(A_WHEEL, T_FABRIC, KAPPA_PET, C_PET, RHO_PET)
restraint_layer = Component(A_WHEEL, T_FABRIC, KAPPA_KEVLAR, C_KEVLAR, RHO_KEVLAR)
abrasive_layer = Component(A_WHEEL, T_FABRIC, KAPPA_1680D_B_NYLON, C_1680D_B_NYLON, RHO_1680D_B_NYLON)
wheel_hub = Component(A_HUB,T_HUB,KAPPA_6061T6,C_6061T6,RHO_6061T6,EPSI_6061T6)
comps = [hermetic_layer, restraint_layer, abrasive_layer, wheel_hub]

p_wheel = 137895

m_argon = V_WHEEL* p_wheel / 8.314 / T_0 * 0.40

A_proj = r * (R+r)*4
Q_WHEEL_ASSY = epsi_default*A_proj* Q_SUN

MC = np.sum([comp.mc() for comp in comps]) + m_argon * C_ARGON
t = 7*1.5*60*60 # 1.5x operating time

DT = Q_WHEEL_ASSY / MC * t

print(f"MAX TEMPERATURE OF WHEELS: {20 + DT} C")
dP = m_argon /MOL_MASS_ARGON*8.314 * (T_0+DT)/V_WHEEL
print(f"MAX PRESSURE CHANGE OF BODY: {dP/6895-20} PSI")

#### BODY

A_EBAY = np.pi * 0.35**2/2 + np.pi*0.35*0.10 # close face, 35cm D cylinder
t_EBAY = 0.005

```

```

A_RODS = 0.03175*4*1.2 # 3.175 cm square rods, expand to 1.2 m
t_ROD = 0.274
A_BODY = 0.1778*np.pi*1 # 1 m 18 cm D cylinder (apprx)
V_BODY = (0.1778/2)**2*np.pi*1
P_BODY = 241317

ebay = Component(A_EBAY,t_EBAY,KAPPA_6061T6, C_6061T6,RHO_6061T6,EPSI_6061T6)
hermetic_body = Component(A_BODY, T_FABRIC, KAPPA_PET, C_PET, RHO_PET)
restraint_body = Component(A_BODY, T_FABRIC, KAPPA_KEVLAR, C_KEVLAR, RHO_KEVLAR)
abrasive_body = Component(A_BODY, T_FABRIC, KAPPA_1680D_B_NYLON, C_1680D_B_NYLON, RHO_1680D_B_NYLON)
tel_rods = Component(A_RODS,t_ROD,KAPPA_6061T6,C_6061T6,RHO_6061T6,EPSI_6061T6)
m_argon = V_BODY*P_BODY / (8.314*T_0)*0.4
MC_bod = 2*ebay.mc() + 3 * tel_rods.mc() + hermetic_body.mc() + restraint_body.mc() + abrasive_body.mc()
A_proj_body = .1778 * 1

Q_body_active = epsi_default*A_proj_body*Q_SUN + 2*Q_MOTOR_RUNNING
Q_body_idle = epsi_default*A_proj_body*Q_SUN + 2*Q_MOTOR_IDLE
time_idle = 5*60*60*1.5
time_running = 2*60*60*1.5

DT_bod = Q_body_active/MC_bod * time_running + Q_body_idle/MC_bod*time_running
dP_body = m_argon /MOL_MASS_ARGON*8.314 * (T_0+DT)/V_BODY
print(f"MAX TEMPERATURE OF BODY & ELECTRONICS: {20 + DT_bod} C")
print(f"MAX PRESSURE CHANGE BODY: {(dP_body- P_BODY)/6895} PSI")

# REFERENCES
# [1] https://www.matweb.com/search/datasheet.aspx?MatGUID=a696bdcdf6f41dd98f8eec3599eaa20&ckck=1
# [2] https://www.matweb.com/search/datasheet.aspx?MatGUID=77b5205f0dcc43bb8cbe6fee7d36cbb5
# [3] https://www.matweb.com/search/datasheettext.aspx?matguid=a2e79a3451984d58a8a442c37a226107
# [4] https://www.matweb.com/search/datasheet.aspx?MatGUID=b8d536e0b9b54bd7b69e4124d8f1d20a

```

## 8.1 Results

- Max temperature of wheels: 117 C
- Max pressure change of wheels: 6.7 PSI
- Max temperature of body and electronics: 84 C
- Max pressure change of body: 11.6 PSI

## Appendix B: Structural Analysis

For brevity, this report only considered the most recent structural analysis. Analyses, both analytical and computational, were done throughout the proposal and design process to aid the decision making process. This analysis considered the robustness of the system against torsion and the robustness of the system against load from cargo. It did not consider the coupled dynamics of these effects. Due to the complex nature of the system and the high level of uncertainty in existing methods to computationally validate inflatable softgoods structures, FEA or hand calculations alone cannot provide results with high confidence for this system. Thorough experimental testing would be required to properly bound the operational range of Cargo-BEEP. Due to time and cost constraints, FEA was accepted to justify the final prototype's design, and these concerns were mitigated with high safety margins.

### Appendix B.1 Static Load From Cargo

The set up for the analysis is shown in Figure A.1. A 20 psi pressure load was applied to the rims and the cargo weight was distributed across the inflatable body. All components were assumed to be made of steel, as this was the material most readily available to our team. The results of this analysis strongly suggest that lighter materials such as aluminum could be substituted with additional validation. Gravity was activated for the model. The connecting interfaces (e.g. wheel shaft, standoffs) were bonded along the mating surfaces. The rods were not included as they are purely to provide torsional resistance.

The results for statically loading Cargo-BEEP with various loads are summarized in Table A.1. The required cargo capacity of cargo-BEEP is 300 kg. This analysis demonstrates Cargo-BEEP can withstand this static load with a safety factor of 3.6. Additionally, the high-stress values occur at concentrations around bolt holes, and some of them may be FEA artifacts.

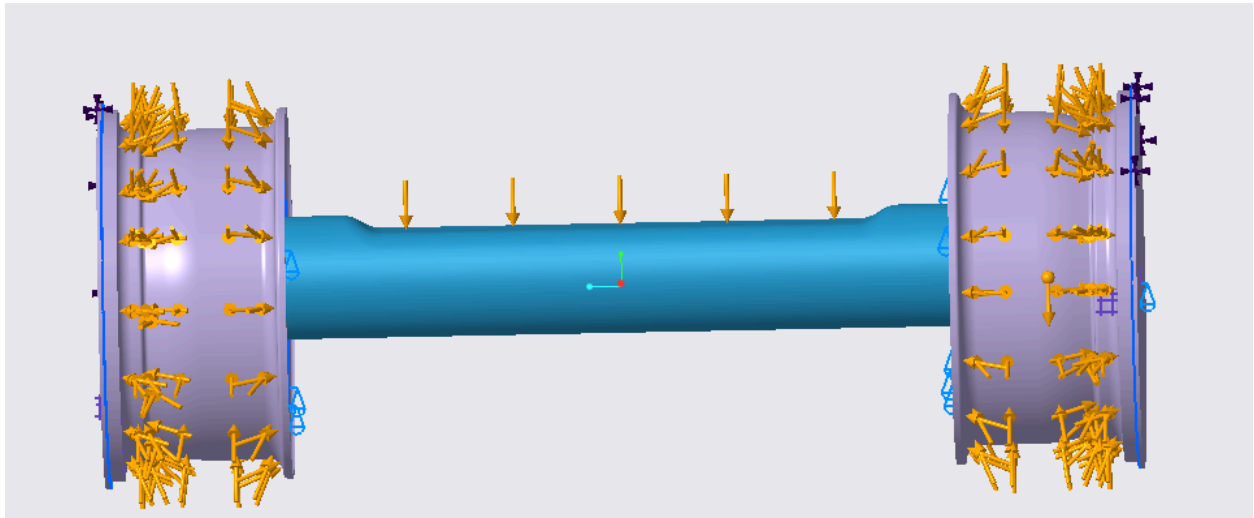


**Figure B.1.** Set up for structural analysis to validate cargo-carrying ability. The wheels were clamped at the top half of the rim as this maximized the stresses observed and the exact dynamics of the system with loads applied are uncertain.

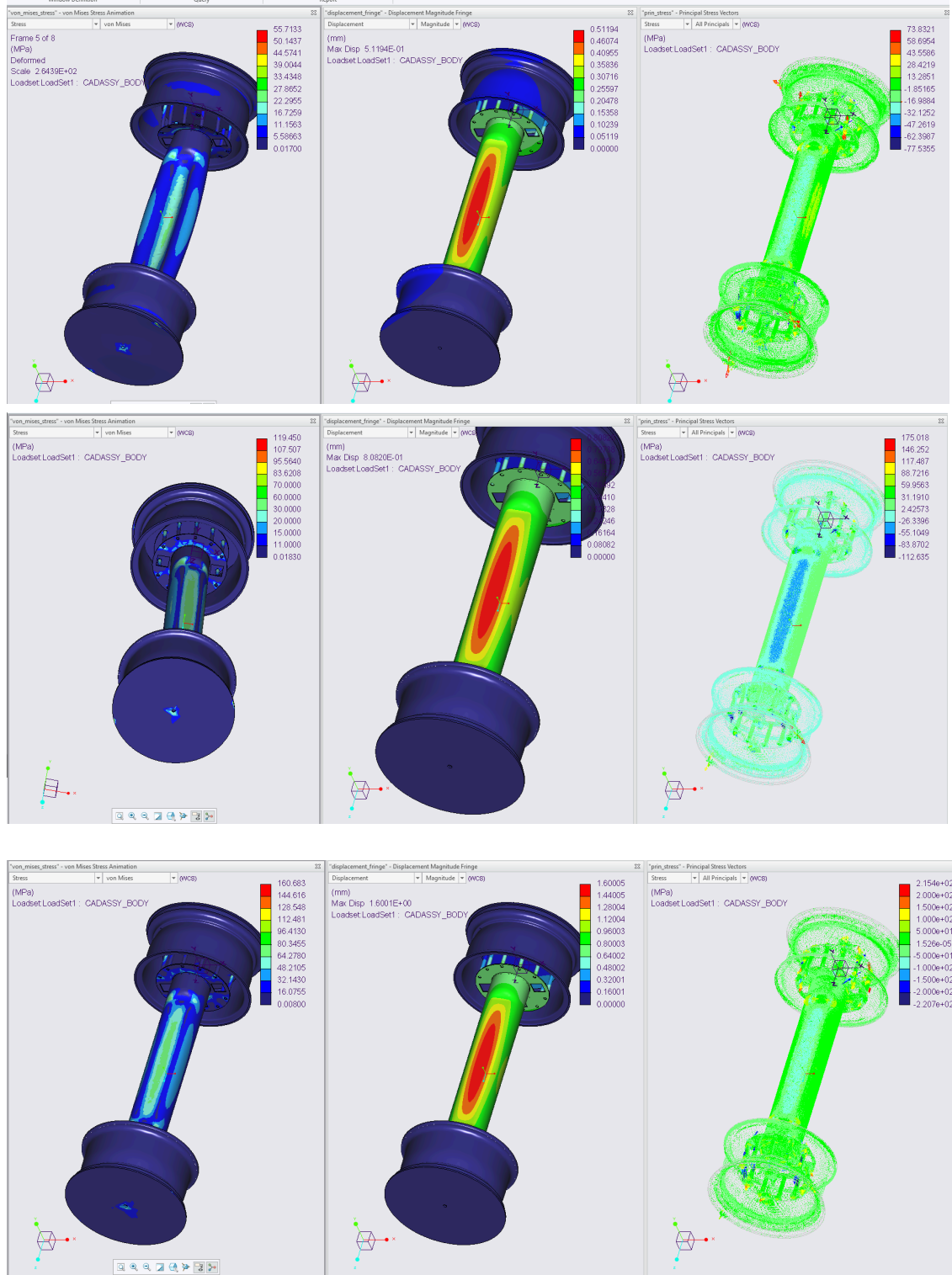


**Figure B.2** Structural analysis results for 300 kg (Top) 500 kg (Center) and 1000 kg (Bottom)

## Appendix B.2 Torsional load from motors

Cargo-BEEPs inflatable center body does not resist torsion, and twists when a torsional load is applied. While the Kevlar is strong enough to be undamaged by this, it poses a serious controls issue and could cause cargo to fall off. It is therefore necessary to include support rods to resist the twist. These rods each consist of 4 rod segments which telescope to extend. They are locked with fasteners once expanded as illustrated in Figure A.2. The body was not included in this simulation. The rods were bonded to the face of the e-bay, and the welded stringers were bonded to the rods. The locking mechanism was modeled as bolt fasteners in Creo. 18 N-m was applied through each shaft, and one wheel rim was clamped. A static structural analysis was then performed. The maximum stress experienced by the rods was 153 MPa, below the yield stress of the materials by 50 MPa. Note that this is a highly conservative estimation and the motors would be unable to sustain such a load without rapidly burning out.

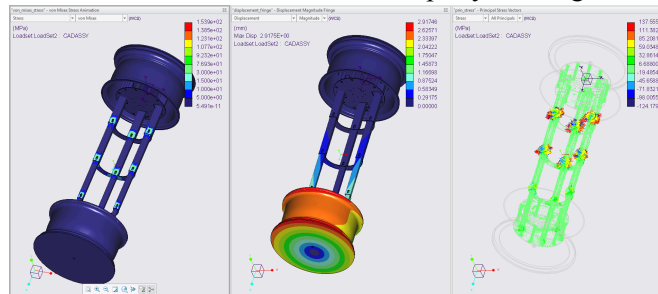


Figure B.3. Torsional load from motors.

## Appendix C: References

- [1] “Lunar Mobility Drivers and Needs”, NASA, 2024. Available: <https://www.nasa.gov/wp-content/uploads/2024/06/acr24-lunar-mobility-drivers-and-needs.pdf?emrc=b2dafa>
- [2] “Lunar Surface Cargo”, NASA, 2024. Available: <https://www.nasa.gov/wp-content/uploads/2024/06/acr24-lunar-surface-cargo.pdf?emrc=641f61>
- [3] G. Valle, D. Litteken, and T. Jones, “Review of Habitable Softgoods Inflatable Design, Analysis, Testing, and Potential Space Applications,” American Institute of Astronautics. Accessed: Oct. 16, 2024. [Online]. Available: [ntrs.nasa.gov/api/citations/20190000847/](https://ntrs.nasa.gov/api/citations/20190000847/)
- [4] Raboin, G. Spexarth, and G. Valle, “TransHab Tapered Diamond Stitch Methods Crewed Inflatable Softgoods Structures,” National Aeronautics and Space Administration, Houston, Texas, Aug. 2022. Available: [https://ntrs.nasa.gov/api/citations/20220012860/downloads/TM%E2%80%939320220012860\\_TransHab\\_Tapered\\_Diamond\\_Stitch\\_Methods\\_R1.pdf](https://ntrs.nasa.gov/api/citations/20220012860/downloads/TM%E2%80%939320220012860_TransHab_Tapered_Diamond_Stitch_Methods_R1.pdf)
- [5] P. Berghardt, “Bally Ribbon Kevlar Quote,” *Email Quotation*, Aug. 30, 2024.
- [6] opensourceleg, 2023. <https://www.opensourceleg.org/>
- [7] A. Daca, D. Tremblay, and K. Skonieczny, “Experimental evaluation of cone index gradient as a metric for the prediction of wheel performance in reduced gravity,” *Journal of Terramechanics*, vol. 99, pp. 1–16, Oct. 2021, doi: <https://doi.org/0022-4898>.
- [8] Rosenburg, M. A., O. Aharonson, J. W. Head, M. A. Kreslavsky, E. Mazarico, G. A. Neumann, D. E. Smith, M. H. Torrence, and M. T. Zuber (2011), Global surface slopes and roughness of the Moon from the Lunar Orbiter Laser Altimeter, *J. Geophys. Res.*, 116, E02001, doi:10.1029/2010JE003716.
- [9] K. Wright, “The Ultimate UTV Paddle and Sand Tire Guide,” *SuperATV*, Sep. 28, 2022. <https://www.superatv.com/offroad-atlas/the-ultimate-utv-paddle-and-sand-tire-guide>
- [10] Standard Test Method for Slow Rate Penetration Resistance of Flexible Barrier Films and Laminates. West Conshohocken, PA: American Society for Testing and Materials. Available: <https://www.google.com/url?q=https://www.astm.org/f1306-21.html>
- [11] The Wave Field. Accessed: Oct. 16, 2024. [Image]. Available: [https://campusinfo.umich.edu/sites/default/files/styles/wide/public/2023-04/wave%20field\\_0\\_0.jpg?itok=1w8CRbMY](https://campusinfo.umich.edu/sites/default/files/styles/wide/public/2023-04/wave%20field_0_0.jpg?itok=1w8CRbMY)
- [12] “Gasket Handbook, 1st Edition,” Fluid Sealing Association, European Sealing Association, Jun. 2017. Available: <https://www.fluidsealing.com/wp-content/uploads/FSA-Gasket-Handbook-June-2017.pdf>
- [13] H. de la Fuente, J. Raboin, G. Spexarth, and G. Valle, “TRANSHAB: NASA’s Large-Scale Inflatable Spacecraft,” American Institute of Aeronautics and Astronautics, Atlanta, Georgia, Apr. 2000. Available: <https://ntrs.nasa.gov/api/citations/20100042636/downloads/20100042636.pdf>

[14] Pedley, M, Mayeux, B. TransHab Materials Selection, NASA Johnson Space Center, Aerospace Materials, Processes, & Environmental Technology.  
Available:<https://ntrs.nasa.gov/api/citations/20010067265/downloads/20010067265.pdf>